

List of major changes to manuscript:

- Updated all figures, captions, statistics, and text to reflect comparison to Kohler (2017) atmospheric CO2 records.
- Revised the manuscript as suggested by Reviewer #1 and Andreas Schmittner. Details below, revised sections marked in **bold**.
- Added 10 Lund et al (2014) South Atlantic sites to compilation and throughout manuscript. Compilation is now at 127 sites.
- As suggested by Reviewer #1, we added a “DOI” column to table A1 and a supplemental file called “TableA1_DOI.xlsx and .csv” so readers can find the original source for the records in this compilation. We are continuing to work on formatting this d13C compilation for archival on both NOAA and Pangaea.
- Table A1 was altered by: adding data DOI/URLs, updating references, rearranging records into regions and descending depth within a region, and double checked spatial coordinates for DSA sites (spot checked other sites). Within the manuscript, table A1 has a very small font size to fit the references and DOI/URLs. Hopefully the Copernicus editorial staff can help in later stages.
- The “tracked changes” style comparison is at the end of this document, but the references compiled in a strange way, so the newly added references show up as “?”. In the comments to reviewer responses, we note the section where new citations are added.

Below are details of how we addressed reviewer suggestions, including previous rebuttal and new comments with revised sections marked in **bold**.

We thank referee #1 for their helpful comments and especially for bringing technical issues to the author's attention. Our responses (AC) are listed after a synopsis of referee #1's comments.

R1 1) Age modelling strategy. It is not entirely clear to me, how age models have been created for the individual cores. It seems though, that the age models are all based on a graphic correlation or automated alignment (?) to the stacks provided by Stern and Lisiecki (2014). If so, it is not clear to me why the authors deliberately used a graphic correlation stratigraphy with an error of 1-2 ka, when radiocarbon dates are available, at least for some of the cores. Radiocarbon ages should provide better constraints on the posterior calendar age distributions. It seems that, at least in the tropics, the uncertainties in the reservoir ages are small enough to provide better constraints on age than ages derived from alignment of benthic oxygen isotopes. I recommend that the authors better explain, how they have obtained the age models why they have not (if not) used the individual calendar age distributions of radiocarbon ages that may exist.

AC 1) Thank you for bringing up this important point of discussion. We have clarified these issues during revision of the manuscript text in **Section 4.2 “Stacking”**.

Yes, the age models used here are those developed by Stern and Lisiecki (2014, *Paleoceanography*; hereafter SL14). The SL14 regional age models have 95% confidence intervals of 0.5-2.0 kyr. (A 2-kyr 95% CI width is approximately equivalent to a standard deviation of 0.5 kyr). We did not perform any new $\delta^{18}\text{O}$ alignments or other age model development for this study.

One of the main goals of this paper is to evaluate whether the SL14 age models are accurate enough to reconstruct the timing of global carbon cycle change. In fact, our results demonstrate that the SL14 age models agree well with ice core CO_2 changes which have very well-constrained age models (Monnin et al., 2004; Marcott et al., 2014; Kohler et al., 2017). Research is currently underway to further improve the sediment core age models and their uncertainty estimates, but this work will take 1-2 years and is clearly beyond the scope of the current paper.

Because the reviewer's questions/concerns about our method will likely be shared by many readers, we will add more explanation of how the SL14 age models were created and why we expect them to have similar or better precision than most ^{14}C age models (i.e., except for a handful of low-latitude cores with the most ^{14}C dates). For example, recent work by Khider et al. (2017, *Paleoceanography*) demonstrates that, for 17 tropical Pacific cores, the uncertainties between radiocarbon ages and $\delta^{18}\text{O}$ alignments are very similar.

Here is the proposed text to add:

Stern and Lisiecki (2014) created seven regional age models based on all available ^{14}C planktonic dates from each region. Each of the seven regions has an age model based on planktonic ^{14}C measurements from multiple cores; ^{14}C dates are combined across cores by assuming that benthic $\delta^{18}\text{O}$ is synchronous within each region (but not necessarily between regions). The first step of this process was generating an initial radiocarbon age model for each of 61 cores by using that core's radiocarbon dates, the Bayesian age modeling software Bacon (Blaauw and Christen, 2011), the Marine13 calibration (Reimer et al., 2013), and constant 405 ^{14}C -yr reservoir ages. Bacon was used to estimate ^{14}C -based ages at specified depths throughout each core, including Monte Carlo uncertainty estimates that increase with distance from the ^{14}C measurements. To identify the core-specific depths for which ^{14}C -based ages would be combined, each core's benthic $\delta^{18}\text{O}$ record was aligned to an Atlantic or Pacific target core using the alignment software Match (Lisiecki and Lisiecki, 2002). Creating regional age models maximizes the total number of ^{14}C dates which contribute to each age model. For example, the intermediate Pacific age model is derived from 14 sediment cores that include a total of 160 radiocarbon dates. The $\delta^{13}\text{C}$ records analyzed here use the age models produced by Stern & Lisiecki (2014), which were created by converting each core's Match-based $\delta^{18}\text{O}$ alignment to its region's radiocarbon age model.

Additionally, Stern and Lisiecki (2014) estimate 95% confidence intervals for each regional age model using 10,000 Monte Carlo age samples for each core from Bacon. Age uncertainty estimates for each region include the effects of any errors in benthic $\delta^{18}\text{O}$ alignment because alignment errors would increase scatter in the compiled radiocarbon dates (by aligning portions

of cores with different ages) and, thus, increase the observed spread in age estimates. For the time range of 0-20 kyr used in our $\delta^{13}\text{C}$ compilation, the 95% confidence interval widths of the regional age models range from 0.5-2.0 kyr. Although Match does not quantify alignment uncertainty, alignment uncertainties have been estimated using a similar algorithm, called HMM-Match (Lin et al., 2014). For age models generated either by $\delta^{18}\text{O}$ -alignments or radiocarbon, the amount of age uncertainty depends on the time resolution of the $\delta^{18}\text{O}$ or ^{14}C data, respectively. A comparison of 15 low-latitude Pacific cores found that ^{14}C -based age uncertainty is comparable to, if not greater than, the uncertainty associated with $\delta^{18}\text{O}$ alignments by HMM-Match (Khider et al., 2017, Paleoceanography).

R1 2) ... It is not clear, whether age uncertainty has also been considered when producing the stacks (i.e. through time series ensembles), and (if so) what assumption has been made regarding the distribution of age uncertainty (i.e. normally or uniformly distributed). The authors might argue that the age uncertainty is already included through the averaging of several time-uncertain time series to produce the stacks, but on the other hand the number of time series is small for some of the stacks and perhaps not representative for the error.

AC 2) The contribution of age uncertainty is important to consider. For clarification, **we added a new section 4.3 “Stack limitations and uncertainty”**. Additionally, **in section 4 “Methods”**, we clarified the descriptions of our methods and the sources of uncertainty, including our bootstrapped Monte Carlo uncertainty estimates. Specifically, estimates of 0.1-0.25‰ in foraminiferal $\delta^{13}\text{C}$ estimates implicitly include the effects of age model uncertainty. For example, Marchal and Curry (2008) report a standard deviation of 0.1‰ which “includes errors in sediment core chronology and oceanic representativity of benthic $\delta^{13}\text{C}$, which alone appears better than this value on average”. Additional discussion of the most appropriate $\delta^{13}\text{C}$ uncertainty is presented in response to Q7 of reviewer 2. We have decided to increase the $\delta^{13}\text{C}$ uncertainty to 0.2‰, which will slightly increase our reported uncertainties.

Additionally, we address age model uncertainty by calculating the correlations between our $\delta^{13}\text{C}$ results and ice core CO_2 for a range of time lags. Because age model errors would be expected to weaken the correlation between these two archives, the comparison we present is conservative, and improved age models would likely strengthen the observed correlations. During revision, we will add more discussion throughout the manuscript of the potential impact of age uncertainty.

R1 3) Variations in sea level affect the water depth of the core location by more than 100 m over the considered time period. If core locations are close to the boundary between the intermediate box and the deep box, a core might fall into the shallow box during the LGM and into the deep box at 6 ka. The authors should clearly describe whether water depth always refers to the modern water depth. This is particularly important for figure 2, where apparently LGM and 6 ka symbols have been plotted at the same water depth. Sea level changes should also be taken into account in the animation provided

in the supplement.

AC 3) This is a good point to bring up that will be clarified in the manuscript text in **section 4.2 “Stacking”**. Sea level changes are not included in our volume weighting -- modern sea level and volumes (calculations based on GEBCO 2014, <https://doi.org/10.1002/2015EA000107>) are used throughout the deglaciation because incorporating sea level changes in our calculations would likely introduce undesirable data artifacts in the regional stacks. The depth-boundary between intermediate and deep boxes would need to shift every 1 kyr, and some sites near the boundary would move from an intermediate to deep box across the deglaciation. Because core coverage is relatively sparse, only a few cores would be affected. If we allowed cores to jump between regions as sea level rises, we would alter the spatial representation of cores in the regions, potentially creating artificial jumps in the regional $\delta^{13}\text{C}$ stack when these cores switched regions.

R1 4) Data base documentation: how have the data been aligned to the stacks. Has this just been done by graphic correlation or has some automatic alignment been involved? If the age models are based on an automatic alignment the methods should be clearly stated. If it is just based on individual age markers and interpolation, these markers should also be included into the data set in the supplement.

AC 4) As described in the response to question 1, the age models used here are those developed by Stern and Lisiecki (2014, *Paleoceanography*; hereafter SL14). **Section 4.1** clarifies that we did not perform any new $\delta^{18}\text{O}$ alignments or other age model development for this study. Therefore, aside from a summary of the methods of SL14, no additional age model documentation should be required. The supplemental materials include both core depth and estimated age for each $\delta^{13}\text{C}$ measurement in each core.

R1 5) Real depth vs. composite depth?

AC 5) Details such as composite depth vs. real depth are not always clearly documented when data are downloaded from a repository, but we have done our best to preserve the integrity of the original data. **We document the DOI identifier or URL for each core’s record in Table A1 and in the folder for additional supplemental files “TableA1_DOI.xlsx and .csv”** so that readers will have the ability to find the original documentation for each $\delta^{13}\text{C}$ record used (see next question/reply). Additionally, the distinction between real depth versus composite depth is usually quite small in the top 20-kyr of the record. Regardless of whether real or composite depth is used, our age estimates will be accurate as long as we use the same depth scale that SL14 used when producing their age models. Another indication that the depth scale for each core has been processed in a consistent manner is the observed similarity of $\delta^{13}\text{C}$ records among all cores in each region.

R1 6) I also recommend to document not only the references in table A1, but also the actual source (i.e., PANGAEA, NOAA, personal communication) of the data, if possible with doi. This allows to resolve possible inconsistencies later (see 7/8).

AC 6) We document the DOI or URL for the original data for the records in supplemental table A1 and in the supplemental folder "TableA1_DOI".

Although the reviewer brings up a good point, and outlines what will hopefully become part of the best-practices in our field, we did not keep track of the download location or doi for every site. However, we will try to gather this information for as many of the sites as possible within the time constraints of the manuscript revision. When we finish gathering this meta-data, we will add it to the data compilation that will be uploaded to NOAA and Pangaea.

R1 7-8) Site labels, location info.

AC 7-8) We were able to correct these mistakes. We thank the reviewer for finding inconsistencies in the supplemental files. It is challenging to find every mistake in such a large database without concerted effort. Before submitting the revised manuscript, we will track down and correct any errors in the coordinate information or records from the core sites in this compilation.

We thank referee #2, **Andreas Schmittner** for his comments and improvements to the manuscript. Our responses (AC) are listed after a synopsis of Andreas' comments (R2).

R2 1) I think typically the relationship between the terrestrial carbon storage and whole-ocean $\delta^{13}\text{C}$ changes is calculated using a closed system approach with land, ocean and atmospheric reservoirs of carbon (e.g. page 1, lines 14-15; Ciais et al. 2012). I wonder if this is appropriate for glacial-interglacial changes because it is likely that ocean sediments responded by adding/removing alkalinity and carbon from dissolution/accumulation of calcium carbonate. This would also affect $\delta^{13}\text{C}$ of DIC. Is this considered here? It would be good to discuss this point.

In Figure 5, which relationship between $\delta^{13}\text{C}$ and land carbon was used? See comment above. Does it consider sediment carbon changes?

AC 1) We clarify these points in section 5.1 and figure 5.

Our "global mean $\delta^{13}\text{C}$ " is a volume-weighted average of benthic $\delta^{13}\text{C}$ (per mil). In the discussion, we refrain from converting the $\delta^{13}\text{C}$ estimate to terrestrial carbon storage because it is difficult to propagate errors through the mass balance calculations. To avoid making this conversion, we use two separate y-axes when comparing terrestrial carbon storage change and benthic $\delta^{13}\text{C}$ change in Figure 5. We will modify the text to clarify that the magnitude of carbon storage and benthic $\delta^{13}\text{C}$ change is not necessarily equivalent, and that Figure 5 is not meant to be a quantitative comparison. In this manuscript, we are simply noting the remarkable similarity in the pattern of change between our data compilation and the only model results of

terrestrial carbon storage change across the deglaciation that we were able to find before submission.

R2 2) Benthic $\delta^{13}\text{C}$ is affected by carbonate ion and pressure effects (e.g. Schmittner et al., 2017). Were these effects considered here? I guess not since carbonate ion changes are not available. In this case it may be useful to try one of their regression equations that don't require carbonate ion to calculate $d_{13}\text{C}_{\text{DIC}}$

AC 2) We address this in section 4.3.

That is correct, the effects of carbonate ion are not considered here because estimates of past carbonate ion concentration are currently difficult to constrain. We will make this clear in the revised text and cite the regressions from Schmittner et al. (2017) as way to account for carbonate ion changes if carbonate ion data becomes available or if readers want to consider model-based estimates of carbonate ion concentration. We will also mention the available regressions that can be used when carbonate ion conc. records are unavailable. Because the relevant experiments (LW6 and CW6) suggest a linear scaling of $\delta^{13}\text{C}$ (i.e., do not include a depth-dependent term), applying these regressions would not impact the correlation coefficients in our manuscript. Additionally, we will mention that these regressions would impact the apparent scaling between $\delta^{13}\text{C}$ and terrestrial carbon implied by Figure 5. We prefer not to apply the regression scaling to $\delta^{13}\text{C}$ in this figure because it could confuse readers and cause misinterpretation of our results.

R2 3) Page 8, 21: "DSA $\delta^{13}\text{C}$ begins increasing at 18 ka" This finding seems to be at odds with Lund et al's (2015, doi:10.1002/2014PA002657) findings that the DSA begins increasing only later (after HS1). Are those data included here? Discuss.

AC 3) We added 10 sites from Lund et al. 2015 that were not originally included in the manuscript and used their ^{14}C age models.

The records from Lund et al. (2015) were not originally included in the manuscript because they were published after Stern & Lisiecki (2014) created their original compilation and were not included in their regional stack age models. We have now included 12 of the Brazil Margin sites from Lund et al. (2015) using their ^{14}C age models. This doesn't change our overall results or the timing of $\delta^{13}\text{C}$ changes in the DSA region. The DSA $\delta^{13}\text{C}$ value at the LGM is slightly more depleted than the original version without these sites, but the timing of deglacial increase is visually similar to before. We didn't do any formal change point analysis to quantify the timing of $\delta^{13}\text{C}$ changes because the focus of this paper is on comparing the global $\delta^{13}\text{C}$ gradient with the ice core CO_2 record throughout the entire deglacial transition.

R2 4) Page 9, 13: The North Pacific (>30N) is also not included. Page 10, 9: what volume was used for the deep Pacific box? <30N?

AC 4) We have two Pacific records at ~32N (one each in the intermediate and deep Pacific regions), but none further north. However, our Pacific volume estimates are based on the latitude range of 60S to 60N. Therefore, the North Pacific (>30N) is volumetrically included but not well constrained.

We are aware of efforts currently underway to compile and publish North Pacific $\delta^{13}\text{C}$ records, and we expect these data will slightly alter mean global $\delta^{13}\text{C}$ estimates. However, our compilation and its comparison to ice core CO_2 provides an important scientific contribution in its current form, and our analyses can be revisited as additional data become available.

R2 5) Page 11, 1-3: Schmittner and Lund (2015, *Climate of the Past*, doi:10.5194/cp-11-135-2015) have suggested a different mechanism. Please consider.

AC 5) Citation added to section 6.3.

We have done our best to include a variety of hypotheses, but the number of possible citations is quite large. On Page 11, 1-3, we will revise the text to include the hypothesis that AMOC shutdown induced a decline of biologically sequestered ocean carbon storage (Schmittner and Lund, 2015).

R2 6) Page 5, 9-11: include study by Schmittner and Somes (2016, *Paleoceanography*, doi:10.1002/2015PA002905)

AC 6) Citation added to section 2.3.

Thank you for the suggestion, we will include the citation.

R2 7) Page 7, 12: I didn't find this number (0.15‰ for the standard deviation) in Gebbie et al., (2015). Schmittner et al. (2017) suggest a larger error of ~0.25‰.

AC 7) This is clarified in section 4.3.

The error estimate of 0.15‰ we used is actually a compromise between the errors reported by Gebbie et al. (2015)'s 0.20‰ and Marchal and Curry (2008)'s 0.10‰. However, during revision we plan to change our uncertainty estimate to 0.20‰, which will increase our stack 95% confidence intervals by +/- 0.02‰. An uncertainty of 0.20‰ will also be approximately consistent with Schmittner et al. (2017); we will add this citation and an explanation of why the value of 0.20‰ was selected. Specifically, the most relevant uncertainty from Schmittner et al. (2017) would likely be a standard deviation 0.22‰ as observed in experiments LW6 and CW6 in Table 2 of that paper because those experiments are the ones that include only *C. wuellerstorfi*. To the extent that modern-day observations also contribute uncertainty in comparison with late Holocene $\delta^{13}\text{C}$, 0.20‰ is a reasonable estimate of the uncertainty contribution from foraminiferal $\delta^{13}\text{C}$. Additionally, the largest discrepancies between foram $\delta^{13}\text{C}$ and DIC $\delta^{13}\text{C}$ in Schmittner's compilation (their Figure 4) comes from shallow cores (<1 km) and high-latitude regions (especially the Arctic), which are not included in our compilation.

Deglacial carbon cycle changes observed in a compilation of ~~117~~127 benthic $\delta^{13}\text{C}$ time series (20-6 ka)

Carlye Peterson^{1,2} and Lorraine Lisiecki²

¹Department of Earth Sciences, University of California Riverside, Riverside, California, USA.

²Department of Earth Science, University of California Santa Barbara, Santa Barbara, California, USA.

Correspondence: CARLYE PETERSON (CARLYE.PETERSON@GMAIL.COM)

Abstract. We present a compilation of ~~117~~127 time series $\delta^{13}\text{C}$ records from *Cibicides wuellerstorfi* spanning the last deglaciation (20-6 kyr) and well-suited for reconstructing large-scale carbon cycle changes, especially for comparison with isotope-enabled carbon cycle models. The age models for the $\delta^{13}\text{C}$ records are derived from regional planktic radiocarbon compilations (Stern and Lisiecki, 2014). The $\delta^{13}\text{C}$ records were stacked in nine different regions and then combined using volume-weighted averages to create intermediate, deep, and global $\delta^{13}\text{C}$ stacks. These benthic $\delta^{13}\text{C}$ stacks are used to reconstruct **mean**-changes in the size of the terrestrial biosphere and deep ocean carbon storage. The timing of change in global mean $\delta^{13}\text{C}$ is interpreted to indicate terrestrial biosphere expansion from 19-6 ka. The $\delta^{13}\text{C}$ gradient between the intermediate and deep ocean, which we interpret as a proxy for deep ocean carbon storage, matches the pattern of atmospheric CO_2 change observed in ice core records. The presence of **distinet signals from** signals associated with the terrestrial biosphere and atmospheric CO_2 **suggests** indicates that the compiled $\delta^{13}\text{C}$ records have sufficient spatial coverage and time resolution to accurately reconstruct large-scale carbon cycle changes during the glacial termination.

Copyright statement. TEXT

1 Introduction

On glacial-interglacial timescales, carbon cycle changes redistribute the amount of carbon stored in the deep ocean, atmosphere and terrestrial biosphere (*e.g.*, Broecker (1982); Siegenthaler et al. (2005)). For example, as atmospheric CO_2 increased across the deglaciation, atmospheric $\delta^{13}\text{C}$ decreased, likely due to the ventilation of respired, ^{13}C -depleted carbon from the deep ocean (*e.g.*, Schmitt et al. (2012); Eggleston et al. (2016)). However, identifying the biogeochemical mechanisms associated with these carbon transfers is complicated by a variety of carbon cycle feedbacks (*e.g.*, Archer et al. (2000); Sigman and Boyle (2000); Peacock et al. (2006); Toggweiler et al. (2006); Kohfeld and Ridgwell (2009); Brovkin et al. (2012); Menviel et al. (2012); Galbraith and Jaccard (2015); Buchanan et al. (2016)). This study seeks to improve our understanding of glacial-interglacial carbon cycle changes by reconstructing changes in mean ocean $\delta^{13}\text{C}$ and its vertical gradient and comparing the results with changes in the terrestrial biosphere and atmospheric CO_2 .

The $\delta^{13}\text{C}$ of benthic foraminiferal calcite is a well-established carbon cycle proxy, which records the $\delta^{13}\text{C}$ signature of the dissolved inorganic carbon (DIC) in seawater at seafloor depths (e.g., [Woodruff and Savin \(1985\)](#); [Zahn et al. \(1986\)](#); [Lutze and Thiel \(1989\)](#)). Averages of benthic foraminiferal $\delta^{13}\text{C}$ time series, called stacks, can improve the signal-to-noise ratio of regional or global seawater changes (e.g., [Lisiecki et al. \(2008\)](#); [Lisiecki \(2014\)](#)). Global mean benthic $\delta^{13}\text{C}$ change is likely caused by changes in terrestrial organic carbon storage ([Shackleton, 1977](#); [Curry et al., 1988](#); [Duplessy et al., 1988](#); [Ciais et al., 2012](#); [Peterson et al., 2014](#)), while vertical $\delta^{13}\text{C}$ gradients may record changes in deep ocean carbon storage and atmospheric CO_2 ([Oppo and Fairbanks, 1990](#); [Flower et al., 2000](#); [Hodell et al., 2003](#); [Lisiecki, 2010](#)). The vertical $\delta^{13}\text{C}$ gradient between the surface (high $\delta^{13}\text{C}$) and deep ocean (low $\delta^{13}\text{C}$) primarily results from the accumulation of low- $\delta^{13}\text{C}$ respired organic carbon in deep water, which temporarily sequesters it from the atmosphere. Conversely, vertical mixing of the ocean will tend to ventilate deep ocean carbon to the surface ocean and atmosphere while simultaneously decreasing the vertical $\delta^{13}\text{C}$ gradient. Therefore, the vertical $\delta^{13}\text{C}$ gradient likely records changes in deep ocean carbon storage, which is an important factor controlling glacial-interglacial changes in atmospheric CO_2 (e.g., [Schmitt et al. \(2012\)](#); [Eggleson et al. \(2016\)](#)).

Here we compile and analyze [117-127](#) high-resolution benthic $\delta^{13}\text{C}$ records from the Atlantic, Pacific, and Indian Oceans spanning the last deglaciation to investigate changes in both the ocean and terrestrial biosphere components of the global carbon cycle. Benthic $\delta^{13}\text{C}$ records are combined into regional stacks, which are then used to construct time series of volume-weighted global mean $\delta^{13}\text{C}$ and the vertical $\delta^{13}\text{C}$ gradient between intermediate and deep waters.

We analyze these stacks to test the following hypotheses:

1. The deglacial pattern of global mean ocean $\delta^{13}\text{C}$ change is a proxy for changes in the size of the terrestrial biosphere. If so, global mean $\delta^{13}\text{C}$ should continue to increase after atmospheric CO_2 levels plateau at 11 ka due to the slower response times for ice sheet retreat and ecosystem change (e.g., [Hoogakker et al. \(2016\)](#); [Davies-Barnard et al. \(2017\)](#)). We compare the reconstructed global mean $\delta^{13}\text{C}$ change with several carbon cycle model estimates of terrestrial biosphere change. Additionally, we evaluate whether deep Pacific $\delta^{13}\text{C}$ correlates with global mean $\delta^{13}\text{C}$ change as previously assumed ([Shackleton et al., 1983](#); [Curry and Oppo, 1997](#); [Lisiecki et al., 2008](#)). This study provides the first opportunity to compare time series of deep Pacific $\delta^{13}\text{C}$ with a volume-weighted global mean $\delta^{13}\text{C}$ stack.
2. Changes in the vertical $\delta^{13}\text{C}$ gradient should closely resemble time series of atmospheric CO_2 if the deglacial CO_2 increase is caused by a decrease in deep ocean carbon storage. This hypothesis is supported by findings on orbital timescales using a smaller number of sites ([Oppo and Fairbanks, 1990](#); [Flower et al., 2000](#); [Hodell et al., 2003](#); [Lisiecki, 2010](#)), but the link between the vertical $\delta^{13}\text{C}$ gradient and CO_2 has not yet been evaluated at millennial timescales or using a global data compilation. Observing such a link would improve our understanding of deglacial atmospheric CO_2 increase and, furthermore, demonstrate that the data compilation presented here has adequate spatial and temporal resolution with sufficiently precise age models to reconstruct millennial-scale changes in [global benthic \$\delta^{13}\text{C}\$. the global carbon cycle.](#)

2 BACKGROUND

2.1 Benthic $\delta^{13}\text{C}$ reconstructions

Measurements of $\delta^{13}\text{C}$ from the calcite tests of epibenthic foraminifera *Cibicides wuellerstorfi* and related species (Schweizer et al., 2009) are commonly used to trace the spatial distribution of nutrients and deep water masses as well as changes in ocean carbon cycling (e.g., ~~Curry et al. (1988); Duplessy et al. (1988); Curry and Oppo (2005); Schmittner et al. (2017)~~). ~~However~~ Curry et al. (1988); Duplessy et al. (1988); Curry and Oppo (2005); ?). Benthic $\delta^{13}\text{C}$ is also slightly influenced (<15%) by changes in carbonate ion concentration of sea water (?). Additionally, the *Cibicides* species *C. kullenbergi* and *C. mundulus*, often measured in deep South Atlantic cores, appear to record more depleted $\delta^{13}\text{C}$ values than *C. wuellerstorfi* (Gottschalk et al., 2016).

Mean $\delta^{13}\text{C}$ ~~change between~~ has been estimated for the Last Glacial Maximum (LGM, 20 ka) and Late Holocene (6-0 ka) ~~has been assessed with using~~ global compilations of *Cibicides wuellerstorfi* $\delta^{13}\text{C}$ records (e.g., Shackleton (1977); Duplessy et al. (1988); Curry et al. (1988); Boyle (1992); Matsumoto and Lynch-Stieglitz (1999); Curry and Oppo (2005); Herguera et al. (2010); Oliver et al. (2010); Hesse et al. (2011); Peterson et al. (2014); Gebbie et al. (2015)). These time slice studies include as many as 500 core sites, but generally undersample portions of the ocean with poor carbonate preservation, low primary productivity, and low sedimentation rates (i.e., the Southern Ocean south of 55S, the Indian Ocean, and the Pacific Ocean). In contrast, some portions of the Atlantic, especially the North Atlantic, are relatively well-sampled with abundant, well-preserved *C. wuellerstorfi*. Therefore, ~~the time evolution of~~ whole-ocean mean $\delta^{13}\text{C}$ change is less well-constrained than Atlantic ~~vertical, zonal, and meridional~~ $\delta^{13}\text{C}$ gradients.

Because deglacial carbon cycle changes ~~occur~~ occurred on millennial to centennial timescales, ~~there is a need for a high resolution~~ (Marcott et al., 2014), observing these changes in the ocean requires a global compilation of high-resolution benthic $\delta^{13}\text{C}$ ~~compilation of globally distributed sites time series~~ on a consistent age model across the glacial termination. Global Previous global compilations of $\delta^{13}\text{C}$ time series ~~tend to~~ focus on orbital-scale responses because their age models are not precise enough to analyze the relative timing of carbon cycle changes during the deglaciation (e.g., Lisiecki et al. (2008)). ~~One~~ For example, Oliver et al. (2010) caution that their global $\delta^{13}\text{C}$ data synthesis, which includes 258 records from many benthic and planktic foraminifera species, ~~is not recommended for analyzing~~ should not be used to analyze $\delta^{13}\text{C}$ changes on timescales of less than 10 kyr due to age model uncertainty and the inclusion of low-resolution records ~~(Oliver et al., 2010)~~. ~~Studies of~~ . Instead, studies of $\delta^{13}\text{C}$ change across the last glacial termination often ~~focus on~~ use local or regional depth transects that contain high-resolution $\delta^{13}\text{C}$ records with good age control (e.g., Sarnthein et al. (1994); Thornalley et al. (2010); Hoffman and Lund (2012); Tessin and Lund (2013); Lund et al. (2015); Oppo et al. (2015); Sikes et al. (2016)). In modeling studies, transient simulations are typically compared to a small number of individual benthic $\delta^{13}\text{C}$ records or regional syntheses, presumably due to the limitations of available global $\delta^{13}\text{C}$ compilations (e.g. Köhler et al. (2005); Brovkin et al. (2007); Köhler et al. (2010)).

2.2 Terrestrial biosphere and mean ocean $\delta^{13}\text{C}$

A portion of the additional carbon released from the deep ocean since the LGM was taken up by the terrestrial biosphere. The transfer of carbon between the terrestrial biosphere and the deep ocean affects the global mean value of benthic $\delta^{13}\text{C}$ because the mean $\delta^{13}\text{C}$ signature of the terrestrial biosphere is significantly more negative (approximately -25‰) than mean ocean $\delta^{13}\text{C}$ (approximately 0‰) (Shackleton, 1977). The change in global mean benthic $\delta^{13}\text{C}$ between the LGM and the Holocene is estimated to be $0.32\text{‰} \pm 0.20\text{‰}$ (Peterson et al., 2014; Gebbie et al., 2015), but the timing of mean benthic $\delta^{13}\text{C}$ change across the deglaciation is not well known.

~~Deglacial changes in~~ The amount of terrestrial carbon storage change (soils and vegetation) can be reconstructed in many ways, including terrestrial vegetation proxies and archives (*e.g.*, pollen, paleovegetation), carbon cycle models (*e.g.*, box models, inverse methods, dynamic global vegetation models, biomization methods, *etc.*), and proxies such as benthic $\delta^{13}\text{C}$, triple oxygen isotopes (Landais et al., 2007), and atmospheric carbonyl sulfide (Aydin et al., 2016). These methods produce estimates of change in terrestrial carbon storage between the LGM and Holocene ~~that vary~~ varying from 200-1900 PgC due to uncertainties and assumptions associated with each method (see discussion and citations within Peterson et al. (2014)).

Due to uncertainties in the total magnitude of change, here we focus on comparing the timing of changes in terrestrial carbon storage and global mean benthic $\delta^{13}\text{C}$. Models simulate rapid increases in terrestrial carbon storage from approximately 19-10 ka, followed by more gradual changes from 10-0 ka (Kaplan et al., 2002; Joos et al., 2004; Köhler et al., 2005). More recently, the potential effects of changes in poorly-constrained carbon reservoirs (beneath ice sheets and on continental shelves) were evaluated using deglacial simulations of biogeophysical and land carbon changes from the HadCM3 General Circulation Model (GCM). The model simulated a rapid increase in terrestrial carbon storage from 20-14 ka, different responses between 14-11 ka depending on the model scenario, and then steady, gradual change from 11-4 ka (Davies-Barnard et al., 2017).

Estimates of global mean benthic $\delta^{13}\text{C}$ are also used to remove global changes from individual $\delta^{13}\text{C}$ records ~~in order~~ to identify patterns of local or regional change, *e.g.*, related to ocean circulation. Because estimates of global mean $\delta^{13}\text{C}$ have only been available for the LGM and Holocene, some studies use deep Pacific $\delta^{13}\text{C}$ time series as a proxy for global mean $\delta^{13}\text{C}$ change (Shackleton et al., 1983; Curry and Oppo, 1997; Lisiecki et al., 2008). Given the large volume and carbon storage capacity of the deep Pacific, its $\delta^{13}\text{C}$ change should be similar in magnitude and timing to the mean ocean $\delta^{13}\text{C}$ change; however, no study has yet confirmed this relationship. For example, low sedimentation rates and poor carbonate preservation in the deep Pacific may limit how well deep Pacific $\delta^{13}\text{C}$ time series resolve changes in mean ocean $\delta^{13}\text{C}$. Additionally, large changes in Atlantic or Indian Ocean $\delta^{13}\text{C}$ could alter the timing of global mean $\delta^{13}\text{C}$ relative to the Pacific. By constructing a global benthic $\delta^{13}\text{C}$ stack, we can now directly compare deep Pacific $\delta^{13}\text{C}$ with global mean $\delta^{13}\text{C}$ change across the deglaciation.

2.3 Vertical gradients in benthic $\delta^{13}\text{C}$

A vertical gradient in the $\delta^{13}\text{C}$ of DIC between surface/intermediate waters and deep water results from a combination of physical, chemical, and biological processes. The air-sea gas exchange of CO_2 between the atmosphere and surface ocean

generates a temperature-dependent fractionation (Lynch-Stieglitz et al., 1995). Biological productivity in the surface ocean preferentially incorporates ^{12}C into organic molecules, leaving ^{13}C -enriched DIC in surface waters. Conversely, deep water becomes depleted in ^{13}C due to remineralization of sinking organic carbon with a $\delta^{13}\text{C}$ signature of approximately -25‰. The accumulation of respired organic carbon in the deep ocean gradually increases deep water's DIC concentration while decreasing its $\delta^{13}\text{C}$ value. Thus, sinking organic carbon simultaneously creates vertical gradients in both $\delta^{13}\text{C}$ and DIC, creating low $\delta^{13}\text{C}$ and high DIC in the deep ocean and high $\delta^{13}\text{C}$ and low DIC in the surface ocean. However, deep water $\delta^{13}\text{C}$ is also affected by the transport of relatively high- $\delta^{13}\text{C}$ North Atlantic Deep Water into the deep Atlantic, where it mixes with low- $\delta^{13}\text{C}$ waters from the Southern Ocean (Talley, 2013).

Numerous $\delta^{13}\text{C}$ records from the well-characterized Atlantic Ocean demonstrate an enhanced vertical $\delta^{13}\text{C}$ gradient between intermediate and deep water during the LGM (*e.g.*, Curry and Lohmann (1982); Curry et al. (1988); Duplessy et al. (1988); Sarnthein et al. (1994); Hodell et al. (2003); Curry and Oppo (2005); Marchitto and Broecker (2006); Herguera et al. (2010)). The less well-sampled Pacific and Indian Oceans also show signs of enhanced stratification at the LGM based on stronger vertical $\delta^{13}\text{C}$ gradients and other nutrient and ventilation proxies (*e.g.*, Kallel et al. (1988); Matsumoto and Lynch-Stieglitz (1999); Matsumoto et al. (2002); Herguera et al. (2010); Lund et al. (2011b); Allen et al. (2015); Sikes et al. (2016)).

Multiple causes have been proposed for stronger vertical $\delta^{13}\text{C}$ gradients during the LGM, including increased surface productivity and export, increased ocean stratification, and changes in preformed $\delta^{13}\text{C}$ in regions of deep water formation (*e.g.*, ~~Matsumoto et al. (2002); Curry and Oppo (2005); Marchitto and Broecker (2006); Lynch-Stieglitz et al. (2007); Marinov et al. (2008b, a);~~ The Matsumoto et al. (2002); Curry and Oppo (2005); Marchitto and Broecker (2006); Lynch-Stieglitz et al. (2007); Marinov et al. (2008b, a); Therefore, the large vertical $\delta^{13}\text{C}$ gradient at the LGM could indicate a strong biological pump and/or weak vertical mixing, either of which would increase deep ocean carbon storage. Although studies do not agree about the relative importance of different mechanisms in creating this vertical gradient, the consensus is that the enhanced vertical $\delta^{13}\text{C}$ gradient at the LGM is consistent with greater deep ocean carbon storage and that this carbon was transferred to the atmosphere and terrestrial biosphere during the glacial termination.

~~On orbital timescales, changes in the intermediate-to-deep vertical $\delta^{13}\text{C}$ gradient closely match atmospheric CO_2 , with weaker vertical $\delta^{13}\text{C}$ gradients corresponding to higher CO_2 levels (Oppo and Fairbanks, 1990; Flower et al., 2000; Hodell et al., 2003; Köhler et al., 2003). This relationship supports the assertion that many of the processes affecting CO_2 also alter the vertical $\delta^{13}\text{C}$ gradient. Model simulations suggest that multiple processes~~ Multiple processes likely contribute to deglacial p CO_2 rise (Bauska et al., 2016), including ocean temperature increase, enhanced Southern Ocean mixing rates (and the role of sea ice) (*e.g.*, Franois et al. (1997); Crosta and Shemesh (2002); Gildor et al. (2002); Hodell et al. (2003); Paillard and Parrenin (2004)), decreased alkalinity and carbon inventories (Yu et al., 2014; Kerr et al., 2017), reduced biological pump (Buchanan et al., 2016), enhanced global ocean circulation (Buchanan et al., 2016), and coral reef growth (*e.g.*, Vecsei and Berger (2004)).

On orbital timescales, changes in the intermediate-to-deep vertical $\delta^{13}\text{C}$ gradient closely match atmospheric CO_2 , with weaker vertical $\delta^{13}\text{C}$ gradients corresponding to higher CO_2 levels (Oppo and Fairbanks, 1990; Flower et al., 2000; Hodell et al., 2003; Köhler et al., 2003). This relationship suggests that many of the processes affecting CO_2 also alter the vertical $\delta^{13}\text{C}$ gradient. Here we evaluate the relationship between atmospheric CO_2 and vertical $\delta^{13}\text{C}$ change at millennial resolution across the deglaciation. It is beyond

the scope of this study to evaluate how much of the change in CO₂ and the vertical $\delta^{13}\text{C}$ gradient at the LGM is associated with specific processes, such as changes in the biological pump (Archer et al., 2003; Köhler et al., 2005; Brovkin et al., 2007; Galbraith and Jaccard, 2015), deep water formation (McManus et al., 2004; Curry and Oppo, 2005) and/or Southern Ocean stratification (Lund et al., 2011b; Burke and Robinson, 2012).

3 Data

This study presents a compilation of ~~117-127~~ previously published benthic $\delta^{13}\text{C}$ time series of *Cibicides wuellerstorfi* in per mil relative to Vienna PeeDee Belemnite (V.P.D.B.) (Figure 1; Table A1). Each record in the compilation spans the time range 20-6 ka. Analysis does not extend after 6 ka because cores from several data-sparse regions were either too low-resolution or missing sediment from 6-0 ka. We only include $\delta^{13}\text{C}$ records with mean sample spacing better than 3 kyr (~~and 87% have a mean sample spacing of less than 2 kyr~~). We excluded any records with sample gaps of 4 kyr or larger and excluded any cores affected by the phytodetritus effect ("Mackensen effect") as assessed by the original authors and the criteria from Peterson *et al.* (2014). We included one *C. kullenbergi* record from the deep South Atlantic (MD07-3076Q) (Waelbroeck et al., 2011) which may record a more negative $\delta^{13}\text{C}$ value than *C. wuellerstorfi* at the LGM (Gottschalk et al., 2016). Additionally, we use some cores with samples labeled "*C. spp*" that may include some *C. kullenbergi* (Table A1).

4 Methods

4.1 ~~Stacking~~Age models

~~Age models for cores were developed by aligning the benthic $\delta^{18}\text{O}$ records to the regional stacks~~

~~For nearly all cores we use the age models of Stern and Lisiecki (2014), which have age models based on regional benthic $\delta^{18}\text{O}$ alignments and seven regional age models. Each of the seven regions has an age model based on planktic foraminiferal ^{14}C ages. Because age model uncertainties are approximately 1-2 kyrs (Stern and Lisiecki, 2014), and some of the $\delta^{13}\text{C}$ records analyzed have sample spacings of 2-3 kyr, our interpretation focuses on $\delta^{13}\text{C}$ features with timescales of about 2 kyr or greater measurements from multiple cores; ^{14}C dates are combined across cores by assuming that benthic $\delta^{18}\text{O}$ is synchronous within each region (but not necessarily between regions). The first step of this process was generating an initial radiocarbon age model for each of 61 cores by using that core's radiocarbon dates, the Bayesian age modeling software Bacon (?), the Marine13 calibration (?), and constant 405 ^{14}C -yr reservoir ages. Bacon was used to estimate ^{14}C -based ages at specified depths throughout each core, including Monte Carlo uncertainty estimates that increase with distance from the ^{14}C measurements. To identify the core-specific depths for which ^{14}C -based ages would be combined, each core's benthic $\delta^{18}\text{O}$ record was aligned to an Atlantic or Pacific target core using the alignment software Match (?). Creating regional age models maximizes the total number of ^{14}C dates which contribute to each age model. For example, we do not expect to reconstruct abrupt changes associated with the onset of the Billing-Allerd or with centennial-scale CO₂ changes (Marcott et al., 2014). Because the intermediate Pacific age model is derived from 14 sediment cores that include a total of 160 radiocarbon dates.~~

The final age model for each core in *Stern and Lisiecki (2014)* was produced by converting from a (transitional) target age model based on benthic $\delta^{18}\text{O}$ alignment to a regional composite radiocarbon age model.

Our compilation also includes $\delta^{13}\text{C}$ ~~record-resolution varies between sites, we interpolate the~~ from 10 South Atlantic cores that were not included in *Stern and Lisiecki (2014)* and for which we used the cores' published radiocarbon age models (?Hoffman and Lund, 2012; Tessin and Lund, 2013; Lund et al., 2015). These cores are denoted with asterisks in Table A1.

Stern and Lisiecki (2014) estimate 95% confidence intervals for each regional age model using 10,000 Monte Carlo age samples for each core from Bacon. Age uncertainty estimates for each region include the effects of any errors in benthic $\delta^{18}\text{O}$ alignment because alignment errors would increase scatter in the compiled radiocarbon dates (by aligning portions of cores with different ages) and, thus, increase the observed spread in age estimates. For the time range of 6-20 kyr used in our $\delta^{13}\text{C}$ ~~records to an even 1-kyr spacing, which introduces an additional source of uncertainty in C compilation, the data. Although combining information from multiple records inherently risks distorting the true ocean state, this risk is counterbalanced by the potential for improved signal-to-noise when estimating regional and global signals. In supplemental material, we provide the original, uninterpolated records from all 117 sites, which could be used for comparison with transient deglacial ocean circulation experiments~~95% confidence interval widths of the regional age models range from 0.5-2.0 kyr. Although Match does not quantify alignment uncertainty, alignment uncertainties have been estimated using a similar algorithm, called HMM-Match (?). For age models generated either by $\delta^{18}\text{O}$ alignment or radiocarbon, the amount of age uncertainty depends on the time resolution of the $\delta^{18}\text{O}$ or ^{14}C data, respectively. A comparison of 15 low-latitude Pacific cores found that ^{14}C -based age uncertainty is comparable to, if not greater than, the uncertainty associated with $\delta^{18}\text{O}$ alignments by HMM-Match (?).

~~We define regions within ocean basins based on the~~

4.2 Stacking

After compiling all 127 records on their previously published age models, we use spatial patterns in benthic $\delta^{13}\text{C}$ to define nine ocean regions, for example, ~~differing based on different~~ LGM $\delta^{13}\text{C}$ values ~~between-for~~ intermediate and deep sites (Figure 2). In the North Atlantic, we separate the intermediate North Atlantic (INA, 0.5-2 km) from the upper deep North Atlantic (UDNA, 2-4 km) and the lower deep North Atlantic (LDNA, >4 km). Because the South Atlantic has fewer records than the North Atlantic (Table 1) and a different vertical $\delta^{13}\text{C}$ structure (Figure 2), we define the intermediate South Atlantic (ISA) as 0.5-2.5 km and the deep South Atlantic (DSA) as >2.5 km. ~~Although a zonal gradient is evident in the intermediate South Atlantic (Figure 1), as also observed by Peterson et al. (2014), we combine all ISA records into a single region because only three sites are available in the east.~~ We separate the Indo-Pacific into four regions: the intermediate Indian (II, 0.5-2 km), intermediate Pacific (IP, 0.5-2 km), deep Indian (DI, >2 km), and deep Pacific (DP, (>2 km). The longitude boundaries between the Atlantic, Indian, and Pacific basins are the same as in Peterson *et al.* (2014). ~~To create regional stacks, we average the interpolated $\delta^{13}\text{C}$ records in each region (Figure 2; Table A1).~~ Most regions contain at least six ~~cores~~sites; however, the intermediate and deep Indian regions each contain only two ~~$\delta^{13}\text{C}$ records~~sites.

~~Although sea level rises globally by about 130-134 m (??) across the deglaciation, the volumetric change associated with deglacial sea level rise is small, less than 3%. Therefore, we use modern water depths and volumes for all sites at all time steps.~~

This preserves the spatial dimensions of the regions and prevents cores near region boundaries from switching between regions during the deglaciation.

~~To calculate an intermediate~~ create regional stacks, we interpolated all benthic $\delta^{13}\text{C}$ records to an even 1-kyr spacing and averaged all records within each region (Figure 2; Table A1). Intermediate, deep, and global mean $\delta^{13}\text{C}$ stacks (Figure 3, Figure 4) , ~~we calculated the volume of water in each region defined above (Table 1) and averaged~~ are calculated by averaging the regional stacks using volume weighting as a percent of total volume ~~(using over~~ a depth range of 0.5-5 km (Table 1). Thus, we represent regions proportional to their volume rather than over-representing well-sampled regions. ~~These global stacks include~~

4.3 Stack limitations and uncertainty

Although our global stack includes benthic $\delta^{13}\text{C}$ records from ~~sites in~~ the Atlantic, Indian, and Pacific Oceans ~~but excludes, it does not include data from~~ the Southern Ocean, Arctic Ocean, ~~and or~~ shallow inland seas. Additionally, ~~this our~~ compilation only includes benthic $\delta^{13}\text{C}$ records from below 0.5 km; ~~therefore, we refrain from interpreting or making assumptions about $\delta^{13}\text{C}$ above 0.5 km. Planktic~~. Although planktic $\delta^{13}\text{C}$ data suggest that mixed layer $\delta^{13}\text{C}$ values may closely track atmospheric $\delta^{13}\text{C}$ change (Eggleston et al., 2016; Hertzberg et al., 2016), we refrain from interpreting or making assumptions about $\delta^{13}\text{C}$ above 0.5 km. It is beyond the scope of the current study to quantify stack uncertainty associated with portions of the ocean which lack *C. wuellerstorfi* $\delta^{13}\text{C}$ time series.

~~We calculate a vertical~~ Uncertainty estimates for $\delta^{13}\text{C}$ gradient ($\Delta\delta^{13}\text{C}_{T-D}$) using the volume-weighted intermediate and deep regional stacks from the Atlantic and Pacific. The Indian Ocean regional stacks are excluded from this vertical gradient calculation because each Indian region includes only two cores, making these regional stacks more susceptible to noise. A global vertical from *C. wuellerstorfi* range from 0.1‰ (?) to 0.22‰ (experiments LW and CW in ?). Accounting for the carbonate ion concentration of seawater can improve the accuracy of benthic $\delta^{13}\text{C}$ (?), but estimates of carbonate ion changes throughout the deglaciation are scarce. In the absence of carbonate ion data, a linear regression can be used to convert between *C. wuellerstorfi* $\delta^{13}\text{C}$ ~~gradient that includes the Atlantic, Indian, and Pacific Oceans ($\text{AIP } \Delta\delta^{13}\text{C}_{T-D}$) is provided in the supplemental materials (Figure A1, Table A2). Additionally, we construct a vertical and DIC $\delta^{13}\text{C}$ (regressions LW6 and CW6 in ?).~~ However, because our study focuses on the timing of $\delta^{13}\text{C}$ change rather than its amplitude, we present all $\delta^{13}\text{C}$ ~~gradient between the intermediate North Atlantic and deep Pacific ($\Delta\delta^{13}\text{C}_{(TNA/2)-DP}$) (Lisiecki, 2010) and compare both representations of the vertical data using the values originally measured in foraminiferal calcite.~~

Interpolating the $\delta^{13}\text{C}$ records to an even 1-kyr spacing introduces an additional source of uncertainty in the data. Although combining information from multiple records inherently risks distorting the true ocean state, this risk is counterbalanced by the potential for improved signal-to-noise when estimating regional and global signals. In supplemental material, we provide the original, uninterpolated records for all 127 sites, which could be used for comparison with transient deglacial ocean circulation experiments. Because age model uncertainties are approximately 1-2 kyrs (Stern and Lisiecki, 2014) and some of the $\delta^{13}\text{C}$ ~~gradient to atmospheric~~ records analyzed have sample spacings of 2-3 kyr, our interpretation focuses on $\delta^{13}\text{C}$ features with

timescales of about 2 kyr or greater. For example, we do not expect to reconstruct abrupt changes associated with the onset of the Bølling-Allerød or with centennial-scale CO₂ change (Marcott et al., 2014).

We estimate stack uncertainty using Monte Carlo simulations that account for the effects of measurement uncertainty and intra-region $\delta^{13}\text{C}$ variability. Specifically, we generate nominal 95% confidence intervals for the stacks using 10,000 bootstrapped iterations that randomly resample $\delta^{13}\text{C}$ records from each region. During the resampling process, we also simulate $\delta^{13}\text{C}$ measurement uncertainty in each record by adding Gaussian white noise with a standard deviation of 0.150.20‰ (Gebbie et al., 2015). ~~Differences in the benthic $\delta^{13}\text{C}$ stack between different~~ Multiple runs of our Monte Carlo simulations, each with 10,000 iterations, ~~is produce differences in the global benthic $\delta^{13}\text{C}$ stack~~ on the order of 0.02‰ at the LGM (20-19 ka) and ~~even smaller for the Holocene(6 ka). It is beyond the scope of the current study to quantify uncertainty associated with portions of the ocean for which there is no available data~~ less during the Holocene.

4.4 Comparison to atmospheric CO₂

To compare the $\delta^{13}\text{C}$ data to atmospheric CO₂ changes from 20-6 ka, we ~~spliced together the atmospheric CO₂ records of Marcott et al. (2014) and Monnin et al. (2004). No correction was necessary to splice these records at 8.9860 ka because the~~ calculate a vertical $\delta^{13}\text{C}$ gradient ($\Delta\delta^{13}\text{C}_{I-D}$) as the difference between the volume-weighted intermediate and deep regional stacks from the Atlantic and Pacific. The Indian Ocean regional stacks are excluded from this vertical gradient calculation because each Indian region includes only two sites, making the Indian regional stacks more susceptible to noise. A global vertical $\delta^{13}\text{C}$ gradient that includes the Atlantic, Indian, and Pacific Oceans (AIP $\Delta\delta^{13}\text{C}_{I-D}$) is provided in the supplemental materials (Figure A1, Table A2). Additionally, we construct an alternate $\delta^{13}\text{C}$ gradient based on the difference between half the intermediate North Atlantic stack and the deep Pacific stack ($\Delta\delta^{13}\text{C}_{(INA/2)-DP}$), analogous to the gradient compared to CO₂ value of 265.45 p.p.m.v. at 8.9855 ka in Monnin et al. (2004) agrees well with the value of 265.2 p.p.m.v. at 8.9730 ka in Marcott et al. (2014) (Figure 5). For quantitative comparison, we down-sampled the spliced-in Lisiecki (2010).

We interpolate a composite ice core CO₂ record by interpolating it (?) to the same 1-kyr resolution of as our benthic $\delta^{13}\text{C}$ stacks -

and calculate correlation coefficients between CO₂ and the vertical gradient of $\delta^{13}\text{C}$. Additionally, we examine the potential for differences in the timing of CO₂ and $\delta^{13}\text{C}$ change that could be caused by lags in the climate system or age model uncertainty. We ~~calculate correlation coefficients for evaluate~~ different potential lags by interpolating the ~~spliced~~ CO₂ record with different time offsets, using lags that range ranging from +1000 yr to -1000 yr in increments of 100 yr. For example, a 100-yr lag in CO₂ relative to the vertical $\delta^{13}\text{C}$ gradient would be represented by comparing $\delta^{13}\text{C}$ values at 6, 7, ... 20 ka with CO₂ values at 5.9, 6.9, ..., and 19.9 ka. Conversely, a CO₂ lead of 100 yr would be suggested if the correlation between the two is maximized for CO₂ values at 6.1, 7.1, ..., 20.1 ka.

Testing the significance of correlations between $\delta^{13}\text{C}$ and CO₂ is complicated by the fact that both time series are autocorrelated, *i.e.*, each data point is highly correlated with the value immediately before or after. To reduce the impact of autocorrelation, we pre-whiten the data by taking the difference between successive 1-kyr samples before calculating the linear correlation and its statistical significance. Our final assessment of the statistical significance of the correlations accounts for the

reduction in the number of degrees of freedom in the data associated with pre-whitening and ~~for~~ allowing time lags between $\delta^{13}\text{C}$ and CO_2 observations.

5 Results

5.1 Comparison to LGM and Holocene reconstructions

~~Although our time series compilation has~~

Although our compilation of $\delta^{13}\text{C}$ time series includes fewer core sites than some previous studies of LGM $\delta^{13}\text{C}$, it preserves the large-scale features of these LGM $\delta^{13}\text{C}$ glacial reconstructions, such as enhanced vertical and meridional Atlantic $\delta^{13}\text{C}$ gradients (Figure 2) (*e.g.*, Curry and Oppo (2005); Peterson et al. (2014)). Vertical $\delta^{13}\text{C}$ gradients at the LGM are strongest in the glacial North Atlantic, closely followed by the glacial South Atlantic (Peterson et al., 2014). ~~Indo-Pacific $\delta^{13}\text{C}$ values are more depleted than North Atlantic $\delta^{13}\text{C}$ values of the same depth.~~ The most depleted $\delta^{13}\text{C}$ values in the compilation are from the high-latitude deep South Atlantic during the LGM, possibly due to inclusion of data from *C. kullenbergi* (Gottschalk et al., 2016). ~~Equatorial deep South Atlantic records at the LGM have~~ Indo-Pacific $\delta^{13}\text{C}$ values for the LGM are similar to equatorial deep Indo-Pacific South Atlantic records of the same depth and more depleted than North Atlantic $\delta^{13}\text{C}$ records values. However, our compilation lacks Indo-Pacific sites deeper than 3.5 km.

At 6 ka the $\delta^{13}\text{C}$ values in this compilation generally resemble the Holocene compilation of ~~Peterson et al. (2014)~~ Peterson et al. (2014). Minor differences could result from Peterson *et al.* (2014) using Holocene data from 6-0 ka and including more sites from the North Pacific sites and ~~more sites~~ from 0.5-1.5 km depth.

5.2 Regional stacks

We create nine regional $\delta^{13}\text{C}$ stacks from 20-6 ka (Figure 3, Table 1). Six of the regional $\delta^{13}\text{C}$ stacks increase steadily from approximately 20-18 ka to 6 ka (LDNA, DSA, II, IP, DI, DP). Small deviations in the ~~trend~~ trends of the Indian $\delta^{13}\text{C}$ stacks are interpreted as noise because these stacks each contain only two ~~cores~~ $\delta^{13}\text{C}$ records. Three Atlantic regions (INA, ISA, UDNA) show a decrease in $\delta^{13}\text{C}$ from approximately 19-15 ka ~~and then,~~ followed by an increase from 14-6 ka, as described in previous studies (*e.g.*, Hodell et al. (2008); Thornalley et al. (2010); Hodell et al. (2010); Lund et al. (2011a); Tessin and Lund (2013); Oppo et al. (2015)). The UDNA $\delta^{13}\text{C}$ stack ~~is briefly similar to~~ has a $\delta^{13}\text{C}$ value between the ISA and LDNA from 20-17 ka, approximately matches the LDNA at 16 ka, and then resembles the ISA stack from 14-6 ka. LDNA $\delta^{13}\text{C}$ is slightly greater than DSA $\delta^{13}\text{C}$ except at 10 ka when the two stacks briefly converge. The DI and DSA $\delta^{13}\text{C}$ values are generally similar across the deglaciation except that the DSA $\delta^{13}\text{C}$ begins increasing at 18 ka while the DI $\delta^{13}\text{C}$ increase begins at 16 ka. The intermediate-depth $\delta^{13}\text{C}$ stacks in the Indian and Pacific Oceans are very similar for most of the time interval.

Across the deglaciation, the vertical $\delta^{13}\text{C}$ gradient weakens in the Atlantic, most noticeably in the North Atlantic (~~where the~~ INA-LDNA $\delta^{13}\text{C}$ gradient decreases from 1.20‰ at 20 ka ~~and to~~ 0.31‰ at 6 ka). Vertical gradients in the Indian and Pacific Oceans

show much less change. The largest spread in $\delta^{13}\text{C}$ values is observed from 20-18 ka, when the intermediate North Atlantic and deep South Atlantic regions differ by ~~1.6‰; this gradient has decreases to 0.471.50‰, a difference which decreases to 0.40‰ at 11-10 by 10 ka.~~ The maximum difference between regions at 6 ka is 0.91‰ between the intermediate North Atlantic (most enriched) and the deep Indian (most depleted).

5.3 Volume-weighted stacks and global mean $\delta^{13}\text{C}$ stack

A global mean $\delta^{13}\text{C}$ stack is constructed by volume weighting all nine regional stacks. However, we construct two different versions of the intermediate and deep $\delta^{13}\text{C}$ stacks, with and without the Indian stacks, because the Indian regions each contain only two records. Both versions of the intermediate and deep stacks show similar trends, but we focus our analysis on the version that uses only the Atlantic and Pacific regions, which should be less susceptible to noise (Figure 4, Table 1). Results for the intermediate and deep $\delta^{13}\text{C}$ stacks that include Indian Ocean are provided in supplemental materials (Figure A1, Table A2).

The volume-weighted intermediate, deep, and global mean $\delta^{13}\text{C}$ stacks increase across the deglaciation, but the magnitude of change is larger for the deep $\delta^{13}\text{C}$ -stack (0.46‰) than the intermediate $\delta^{13}\text{C}$ -stack (0.24‰) (Table 1, Figure 4). We define the vertical $\delta^{13}\text{C}$ gradient, $\Delta\delta^{13}\text{C}_{I-D}$, as the difference between the volume-weighted Atlantic and Pacific intermediate and deep stacks that exclude the data-sparse Indian regions. This gradient ~~is largest at 20 ka (0.40‰) and shrinks~~ has a maximum of 0.41‰ at 18 ka and decreases to 0.24‰ by 6 ka.

The volume-weighted global $\delta^{13}\text{C}$ stack holds nearly steady from 20 to 19 ka at approximately 0.00‰ (95% CI: ~~-0.10 to 0.09~~ -0.13 to 0.12‰ at 19 ka) and then increases from 18-6 ka, reaching a value of ~~0.37~~ 0.39‰ (95% CI: ~~0.26-0.24~~ to 0.49‰) at 6 ka. The change from 20 to 6 ka in the global stack is 0.36‰ (95% CI: ~~0.25 to 0.46~~ 0.23 to 0.50‰), which agrees to within uncertainty with the LGM-to-Holocene mean $\delta^{13}\text{C}$ change estimate of 0.38‰ (95% CI: 0.30 to 0.46‰) estimated for 0.5-5 km from (Peterson et al., 2014) by Peterson et al. (2014). Recall that the mean $\delta^{13}\text{C}$ estimate from our global stack is not quite a whole-ocean $\delta^{13}\text{C}$ estimate because we do not include data from the surface (<0.5 km), Southern Ocean (>65S), or bottom waters (>5 km). Estimates of whole-ocean $\delta^{13}\text{C}$ change are slightly smaller at 0.34‰ (95% CI: 0.15 to 0.53‰) (Peterson et al., 2014) and 0.32‰ (95% CI: 0.12 to 0.52‰) (Gebbie et al., 2015). ~~The because the~~ surface ocean (0-0.5 km) has ~~enriched $\delta^{13}\text{C}$ values with much~~ less deglacial change (Eggleston et al., 2016; Hertzberg et al., 2016).

6 Discussion

6.1 Terrestrial carbon storage and global mean benthic $\delta^{13}\text{C}$

The long-standing explanation for mean benthic $\delta^{13}\text{C}$ change across the deglaciation is an increase in the size of the terrestrial biosphere (Shackleton, 1977; Curry et al., 1988; Duplessy et al., 1988). Here we compare the timing of changes in our global mean $\delta^{13}\text{C}$ stack (*i.e.*, a monotonic increase from 19-6 ka, Figure 4B) with model simulations and other terrestrial biosphere reconstructions.

A carbon isotope-enabled transient model from LPJ-DVGM simulated a mean ocean $\delta^{13}\text{C}$ increase beginning at 21 ka, with the most rapid changes occurring from 17-10.5 ka (Kaplan et al., 2002). In these experiments, the terrestrial biosphere began expanding around 18-16.5 ka (Joos et al., 2004; Köhler et al., 2005) and rapidly increased from 17-9 ka, with 70% of terrestrial carbon storage change occurring before the Holocene (11.5 ka) (Kaplan et al., 2002). ~~In our global $\delta^{13}\text{C}$ stack~~ Similarly, 67% of the ~~change in our global $\delta^{13}\text{C}$ change stack~~ occurs between 19-11 ka while the remaining 33% ~~of $\delta^{13}\text{C}$ change~~ occurs from 11-6 ka.

Simulations from HadCM3 estimated that 45-70% of terrestrial biosphere expansion occurred between 18-14 ka (Davies-Barnard et al., 2017). Dramatically different trends were observed from 14-6 ka in simulations with different assumptions about carbon storage under glacial ice sheets and on continental shelves. The simulation that most closely resembles our global mean $\delta^{13}\text{C}$ stack is the simulation that releases carbon from under ice sheets to the atmosphere and does not accumulate carbon on exposed continental shelves (Figure 5). This simulation is also the only one which agrees with terrestrial carbon storage change estimates of 440 PgC based on whole-ocean mean $\delta^{13}\text{C}$ change (e.g., Peterson et al., 2014).

~~Climate model simulations of the Holocene~~ Holocene simulations using a global pollen synthesis, the biomization method, and ~~vegetation models~~ models of climate and vegetation (HadCM3, FAMOUS, and BIOME4) suggest that the global average area for most carbon-rich megabiomes (i.e., excluding grasslands and dry shrubland) increased from 10-2 ka and net primary productivity increased from 8-2 ka (Hoogakker et al., 2016). This is consistent with our observation that the global mean benthic $\delta^{13}\text{C}$ trend continued until at least 6 ka. Dramatic land use changes from agricultural practices, another potential mechanism for terrestrial carbon change, did not begin until 4.5 ka (Ruddiman and Ellis, 2009). More detailed evaluation of Holocene terrestrial carbon storage changes will require improved spatial coverage for $\delta^{13}\text{C}$ records from 6-0 ka.

6.2 ~~Global mean $\delta^{13}\text{C}$ and deep~~ Deep Pacific and global mean $\delta^{13}\text{C}$

Previous studies have assumed deep Pacific $\delta^{13}\text{C}$ can be used as a proxy for global mean $\delta^{13}\text{C}$ because the deep Pacific constitutes about 30% of the ocean volume and is not strongly affected by shifting water mass boundaries (e.g., Shackleton et al. (1983); Curry and Oppo (1997); Lisiecki et al. (2008)). From 20-6 ka, the global mean and deep Pacific $\delta^{13}\text{C}$ stacks show similar patterns of change (Figure 6) and fall along a tight regression line

$$\delta^{13}\text{C}_{\text{global}} = 1.021 \pm 0.03 \pm 0.06 \pm 0.07\% \times \delta^{13}\text{C}_{\text{DP}} + 0.180 \pm 0.19 \pm 0.01\%$$

The two time series are highly correlated ($r^2=0.99$), which is not surprising because the large volume of the deep Pacific exerts a strong influence on the global mean $\delta^{13}\text{C}$ stack. ~~However, when~~ When the stacks are pre-whitened to account for autocorrelation (Table 2), their correlation ~~falls on the edge of statistical significance is weaker ($r^2=0.47$) but statistically significant ($p=0.05$). The statistical significance of this correlation is likely limited by the relatively short time interval analyzed and/or noise in the deep Pacific stack, which contains only seven $\delta^{13}\text{C}$ records.~~ 0.04

~~A~~ Alternatively, a carbon cycle box model simulated a strong correlation between deep Pacific $\delta^{13}\text{C}$ and CO_2 across several glacial cycles ($r^2=0.96$) (Köhler et al., 2010). The correlation between CO_2 and our deep Pacific $\delta^{13}\text{C}$ stack ~~and CO_2~~ is statistically significant after pre-whitening ($r^2=0.620$, $p=0.010$), but global mean $\delta^{13}\text{C}$ and CO_2 are not ($r^2=0.200$, $p=0.240$). Our compilation of Pacific records is likely insufficient to determine whether deep Pacific $\delta^{13}\text{C}$ correlates better

with global mean $\delta^{13}\text{C}$ or atmospheric CO_2 . This issue could be better resolved using a $\delta^{13}\text{C}$ compilation spanning multiple glacial cycles and including more deep Pacific sites.

6.3 Vertical $\delta^{13}\text{C}$ gradient and atmospheric CO_2

The vertical $\delta^{13}\text{C}$ gradient ($\Delta\delta^{13}\text{C}_{I-D}$) in our compilation resembles the inverse of CO_2 change across the deglaciation (Figure 7), as would be expected if they are both strongly influenced by changes in deep ocean carbon storage (Flower et al., 2000; Oppo and Horowitz, 2000; Hodell et al., 2003). Alternatively, one orbital-scale study found a ~~stronger~~ stronger correlation with CO_2 using the gradient between the deep Pacific and half the INA $\delta^{13}\text{C}$ stack ($\Delta\delta^{13}\text{C}_{(INA/2)-DP}$) Lisiecki (2010). Both vertical $\delta^{13}\text{C}$ gradients ($\Delta\delta^{13}\text{C}_{I-D}$ and $\Delta\delta^{13}\text{C}_{(INA/2)-DP}$) decrease from 18-11 ka over the same time interval that atmospheric CO_2 increases. In contrast, the global mean $\delta^{13}\text{C}$ stack increases at a relatively steady pace from 19-6 ka. Thus, the ~~vertical~~ $\delta^{13}\text{C}$ ~~gradient records~~ gradients record a distinctly different signal than ~~the~~ global mean $\delta^{13}\text{C}$.

The ~~vertical~~ $\delta^{13}\text{C}$ gradients decrease most rapidly across two time steps, 18-17 ka and 12-11 ka. The first change at 18 ka is approximately synchronous with the start of atmospheric CO_2 rise (~~Marcott et al., 2014~~) (Marcott et al., 2014; ?) and a decrease of 0.3‰ in the $\delta^{13}\text{C}$ of atmospheric CO_2 (Eggleston et al., 2016). In the Southern Ocean at 18 ka, proxy records indicate a decrease in aeolian dust deposition accompanied by lower marine productivity (Martínez-García et al., 2009) and a decrease in winter sea ice cover, which likely reduced vertical stratification (Ferrari et al., 2014). The second rapid change in the vertical $\delta^{13}\text{C}$ gradients at 12 ka approximately coincides with rapidly increasing atmospheric CO_2 from 13-11.5 ka and a decrease of 0.1‰ in the $\delta^{13}\text{C}$ of atmospheric CO_2 .

From 11 to 6 ka, atmospheric CO_2 remains nearly constant with a small (approximately 10 ppm) decrease from 11-8 ka. ~~Change in the~~ The vertical $\delta^{13}\text{C}$ gradients ~~is~~ are also relatively steady from 11-6 ka, with a slight increase in both gradients from 9-8 ka. The small decrease in atmospheric CO_2 beginning at 11 ka (Marcott et al., 2014) has been variously attributed to growth of the terrestrial biosphere, sea level rise, and an increase in gas exchange through reduced sea ice cover (Kaplan et al., 2002; Joos et al., 2004; Köhler and Fischer, 2004; Köhler et al., 2005, 2010).

Although CO_2 correlates strongly with both $\Delta\delta^{13}\text{C}_{I-D}$ ($r^2=-0.98-0.96$) and $\Delta\delta^{13}\text{C}_{(INA/2)-DP}$ ($r^2=-0.98-0.96$), we must pre-whiten these time series to remove autocorrelation before assessing the statistical significance of their correlation. At the 95% confidence level, atmospheric CO_2 significantly correlates with both $\Delta\delta^{13}\text{C}_{I-D}$ ($r^2=-0.70$; $p<0.01$ 0.51; $p=0.03$) and $\Delta\delta^{13}\text{C}_{(INA/2)-DP}$ ($r^2=-0.79-0.69$; $p<0.01$) (Figure A1, Table 2). Better correlation with $\Delta\delta^{13}\text{C}_{(INA/2)-DP}$ could be because of better age control and higher resolution $\delta^{13}\text{C}$ records in the INA region than the other intermediate regions. Determining whether the $\Delta\delta^{13}\text{C}_{(INA/2)-DP}$ gradient or the ~~volume-weighted global~~ vertical $\delta^{13}\text{C}$ gradient correlates better with atmospheric CO_2 will require data with better spatial coverage and/or a longer time span.

Because our comparison of the vertical $\delta^{13}\text{C}$ gradient and CO_2 could be affected by ~~differences in timing caused by carbon cycle processes~~ lags within the carbon cycle or age model uncertainty, we additionally investigate whether the correlations between CO_2 and the vertical $\delta^{13}\text{C}$ gradient would be improved by age model shifts (Table 2). The correlation between CO_2 is maximized when $\Delta\delta^{13}\text{C}_{I-D}$ ~~lags CO_2 by 300 years or when~~ lags $\Delta\delta^{13}\text{C}_{(INA/2)-DP}$ ~~leads~~ lags CO_2 by 200-400 years (Table

2), ~~both of which are~~ which is within the age uncertainty of the sediment core age models. Thus, changes in atmospheric CO₂ and vertical $\delta^{13}\text{C}$ gradients appear synchronous to within age model uncertainty.

~~The prevailing processes~~ Processes that potentially explain atmospheric CO₂ change during glacial cycles include the efficiency of the biological pump (Martínez-García et al., 2009; Galbraith and Jaccard, 2015), circulation changes (~~Ferrari et al., 2014; Lacerra~~ or a combination of ~~these and/or other~~ multiple processes (Bauska et al., 2016; Skinner et al., 2017). ~~These~~ Different processes could influence the carbon cycle on different timescales (Bauska et al., 2016; Kohfeld and Chase, 2017) and/or in different regions (e.g., (Gu et al., 2017)) ~~; which could confound and complicate~~ interpretations of which processes are most responsible for atmospheric CO₂ change. However, because both productivity and circulation change would affect the vertical $\delta^{13}\text{C}$ gradient while changing atmospheric CO₂, we interpret our results as supporting the importance of the deep ocean as a reservoir for storing glacial carbon ~~from related to~~ either or both processes. Furthermore, these results support the use of vertical $\delta^{13}\text{C}$ gradients as a proxy for glacial-interglacial CO₂ change on both orbital and millennial timescales (Lisiecki, 2010).

7 Conclusions

We present regional $\delta^{13}\text{C}$ stacks and volume-weighted intermediate, deep, and global mean $\delta^{13}\text{C}$ ~~stack-stacks~~ from a compilation of ~~117-127~~ benthic *C. wuellerstorfi* $\delta^{13}\text{C}$ records, which span 20 to 6 kyr with a mean age resolution better than 2 kyr. Age models are based on $\delta^{18}\text{O}$ alignments to regional stacks with radiocarbon dating ~~;-with-and~~ age model uncertainties ~~for each core-~~ of approximately 1-2 kyr. Our compilation shows spatial patterns in benthic $\delta^{13}\text{C}$ that are similar to higher resolution reconstructions of the Holocene and Last Glacial Maximum. The volume-weighted mean $\delta^{13}\text{C}$ change ~~estimate of estimated from these 127 records is~~ 0.36‰ (95% CI: ~~0.25 to 0.46‰~~) ~~from the 117 cores in this study is 0.23 to 0.50‰~~, similar to the estimate of Peterson *et al.* (2014) for 0.5-5 km based on 480 ~~cores. This compilation also shows spatial patterns records.~~

Importantly, this global compilation of benthic $\delta^{13}\text{C}$ ~~that are similar to higher resolution reconstructions of the Holocene and Last Glacial Maximum time slices-~~

~~The global mean time series also allows us to evaluate the timing of change in the mean and vertical gradient of $\delta^{13}\text{C}$ and compare them with other carbon cycle changes. The volume-weighted global $\delta^{13}\text{C}$ stack is interpreted as recording an increase in the size of the terrestrial biosphere increases from 19 to 6 ka and likely reflects terrestrial biosphere growth, in agreement with modeling studies (Kaplan et al., 2002; Joos et al., 2004) model simulations (Kaplan et al., 2002; Joos et al., 2004; Davies-Barnard et al., 20~~
To constrain the timing of the end of terrestrial biosphere expansion, future work should focus on extending ~~this estimate the global stack~~ through the Late Holocene. Furthermore, ~~the~~ $\delta^{13}\text{C}$ changes from 20 ka to 6 ka suggest that a deep Pacific $\delta^{13}\text{C}$ stack ~~can be used as a proxy for approximates~~ global mean $\delta^{13}\text{C}$ with an offset of ~~0.18‰. Future work should aim to validate this result over one or more glacial cycles and using more deep Pacific records. Both vertical 0.19‰. Vertical~~ $\delta^{13}\text{C}$ gradients ~~;-~~ between intermediate and deep water ($\Delta\delta^{13}\text{C}_{I-D}$) and between the intermediate North Atlantic and deep Pacific ($\Delta\delta^{13}\text{C}_{(INA/2)-DP}$) ~~;-are interpreted are interpreted~~ as proxies for changes change in deep ocean carbon storage. ~~We find that millennial-scale~~ Millennial-scale features in $\Delta\delta^{13}\text{C}_{I-D}$ and $\Delta\delta^{13}\text{C}_{(INA/2)-DP}$ are significantly correlated with atmospheric CO₂ changes from 20-6 ka.

Based on these [comparisons](#)[analyses](#), we conclude that the four-dimensional compilation of globally distributed $\delta^{13}\text{C}$ time series presented here provides useful constraints for global carbon cycle reconstructions and for comparison with deglacial simulations from isotope-enabled Earth systems models.

Data availability. The original data and publication citations along with this data synthesis are made available in supplemental files.

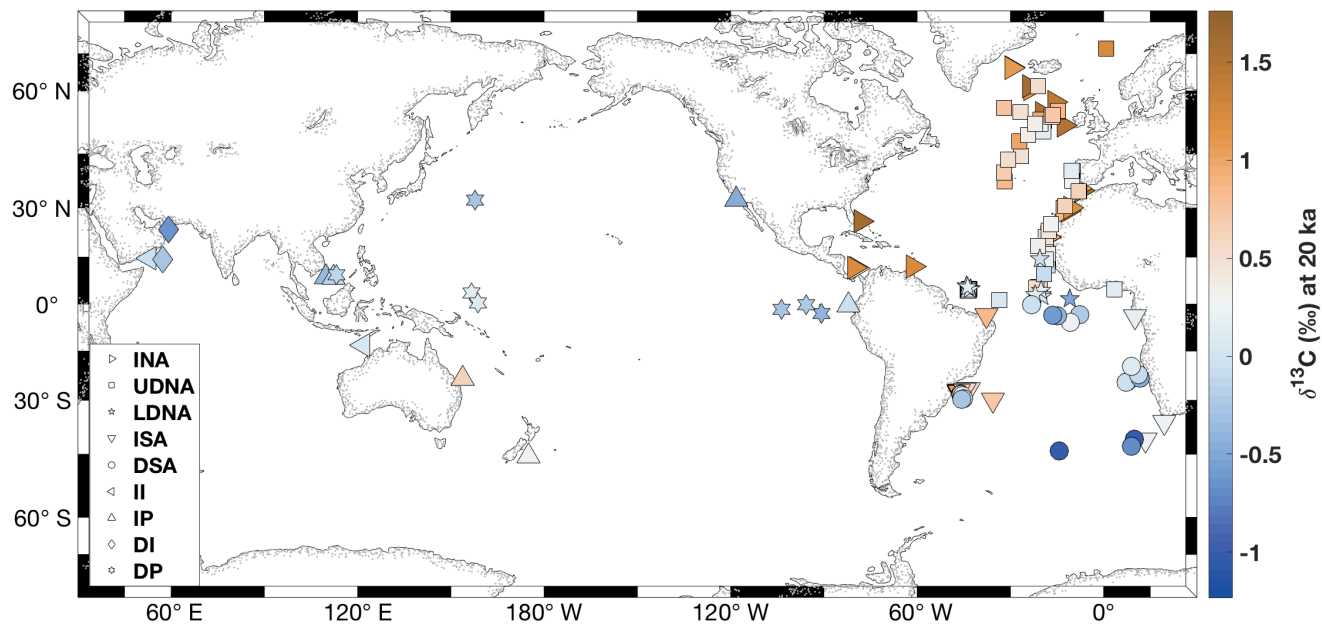


Figure 1. Locations of [117-127](#) core sites compiled for this study, color coded by LGM $\delta^{13}\text{C}$ estimates at each core site. Markers indicate locations of cores in the nine regions: INA = intermediate North Atlantic; UDNA = upper deep North Atlantic; LDNA = lower deep North Atlantic; ISA = intermediate South Atlantic; DSA = deep South Atlantic; II = intermediate Indian; DI = deep Indian; IP = intermediate Pacific; DP = deep Pacific.

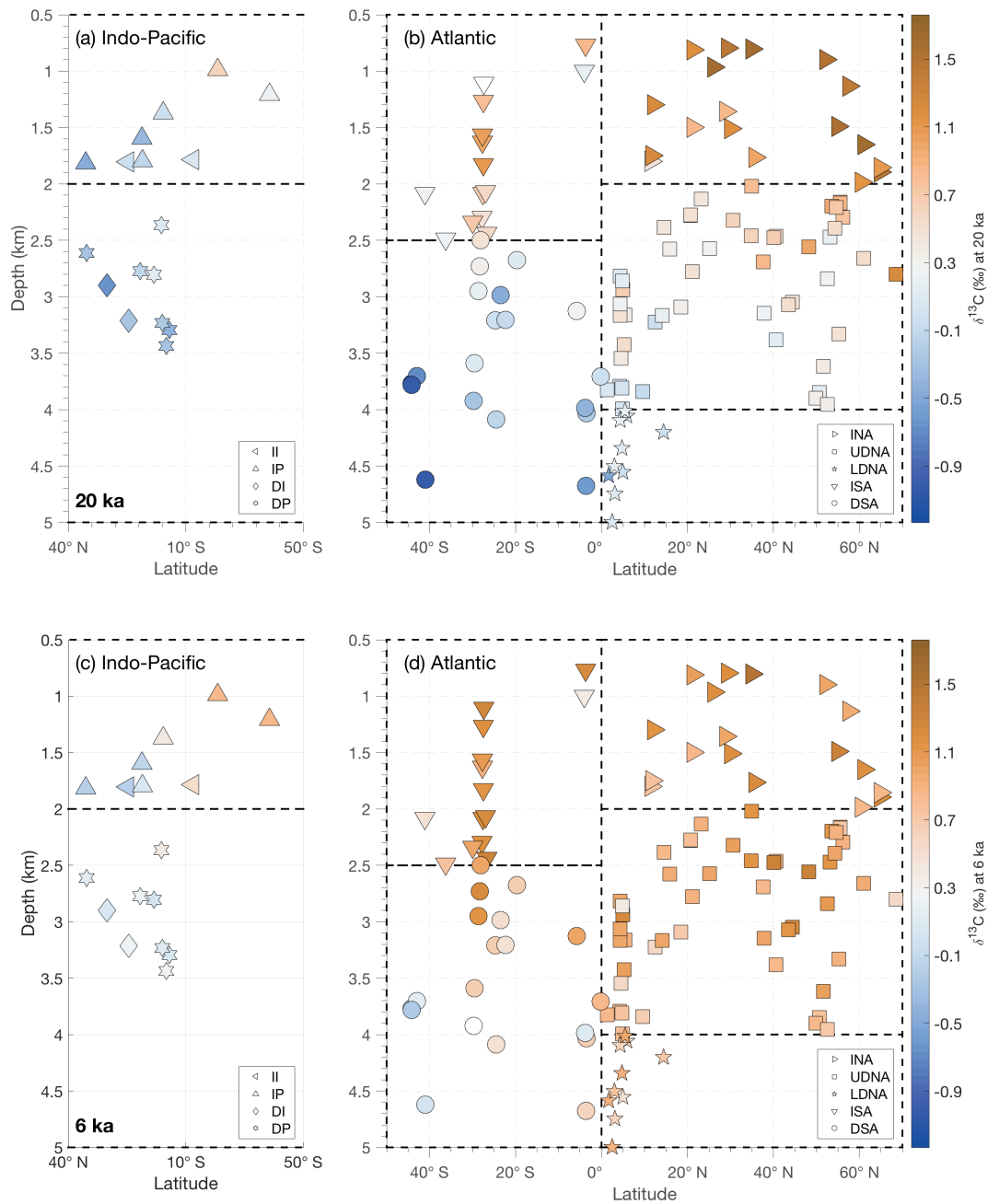


Figure 2. The three-dimensional structure of $\delta^{13}\text{C}$ in Indian and Pacific Oceans (**A-a** and **C-c**) and Atlantic (**B-b** and **D-d**) shown as zonally collapsed cross sections (latitude vs. [modern water](#) depth) with the same marker scheme as in Figure 1. Dotted lines indicate region boundaries. Colors show the $\delta^{13}\text{C}$ value at each site for the LGM (20 ka, top row) and Holocene (6 ka, bottom row). Note that latitudes on the x-axis are oriented so the Southern Ocean is in the center of the figure. Additional time slices (in 1-kyr intervals from 20-6 ka) and an animation of deglacial $\delta^{13}\text{C}$ changes can be found in the supplemental materials.

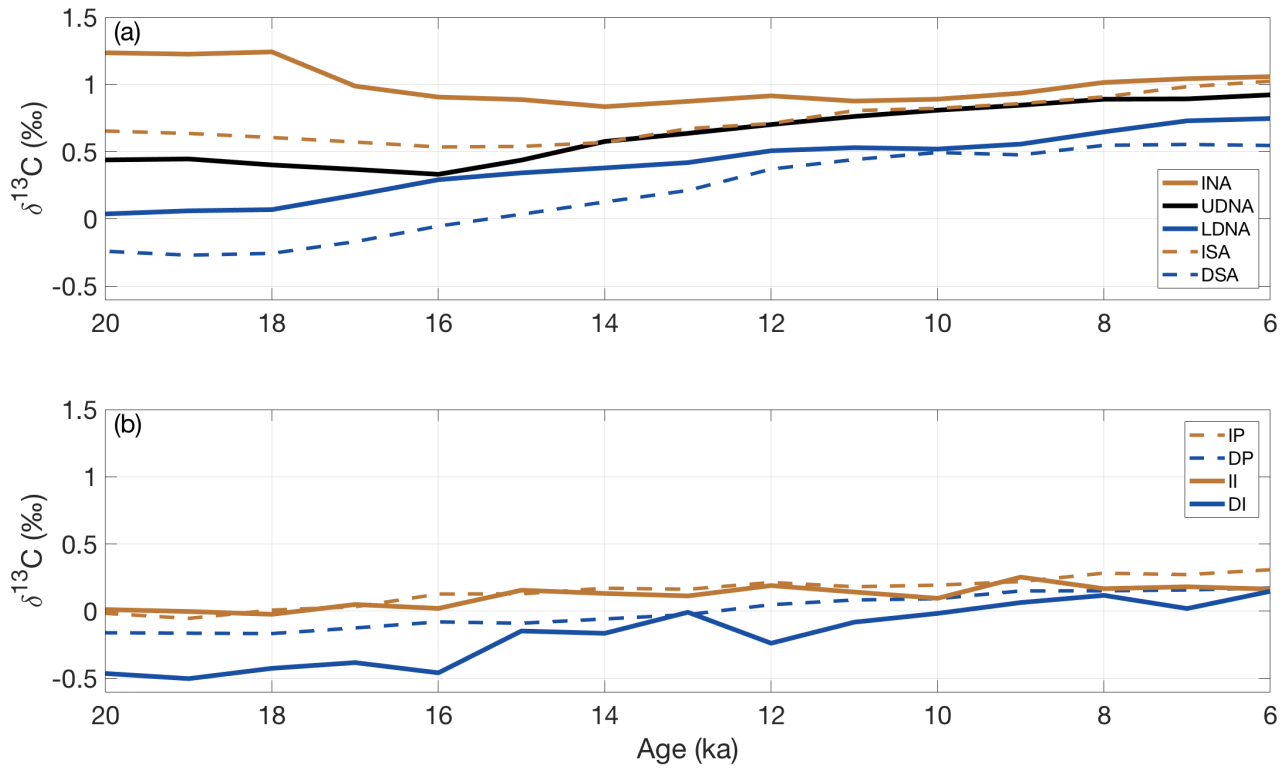


Figure 3. Regional stacks for the (Aa) Atlantic and (Bb) Indian and Pacific Oceans. Note the x- and y-axes are identically scaled. INA = intermediate North Atlantic; UDNA = upper deep North Atlantic; LDNA = lower deep North Atlantic; ISA = intermediate South Atlantic; DSA = deep South Atlantic; II = intermediate Indian; DI = deep Indian; IP = intermediate Pacific; DP = deep Pacific.

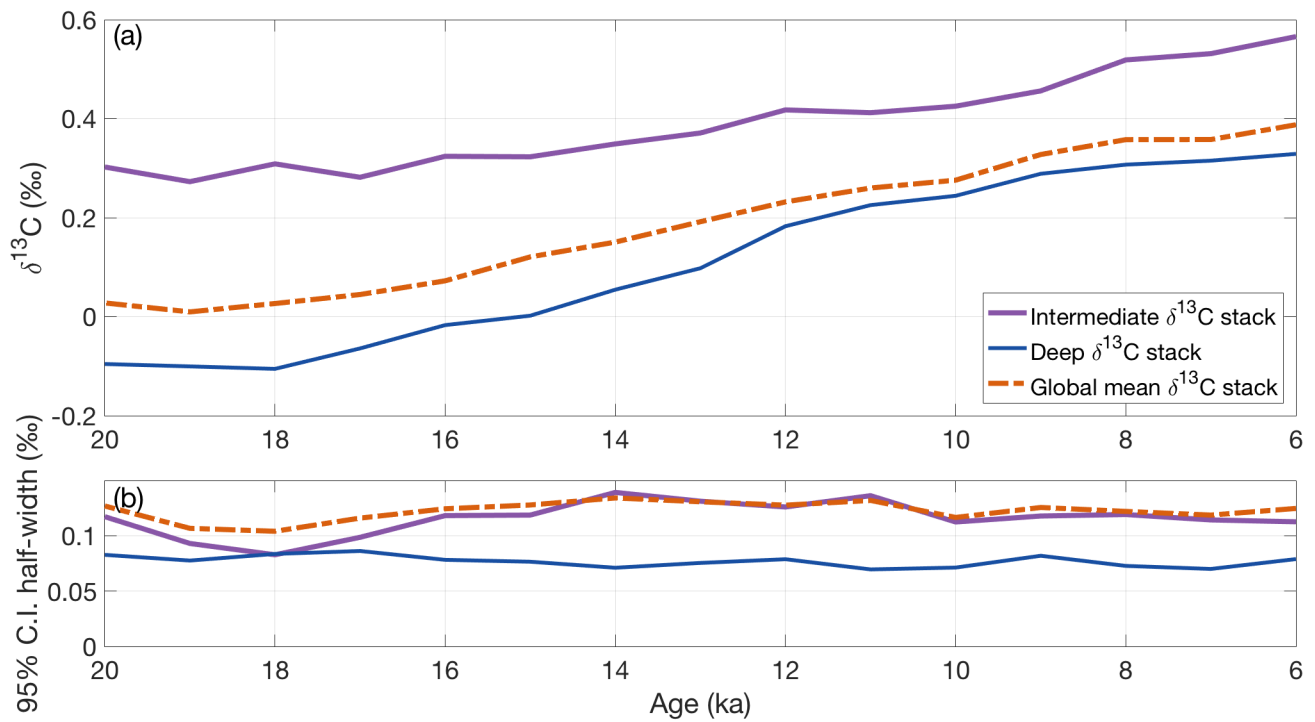


Figure 4. Volume-weighted stacks. **(Aa)** The volume-weighted global stack is calculated based on all nine regional stacks. However, the intermediate and deep stacks shown here only include Atlantic and Pacific data due to the small amount of Indian data. A comparison of these stacks with ones which include the Indian stacks is provided in Figure A1. **(Bb)** Stack uncertainty as characterized by the 95% confidence interval half-width ~~showing the change in uncertainty across the deglaciation for of~~ each stack.

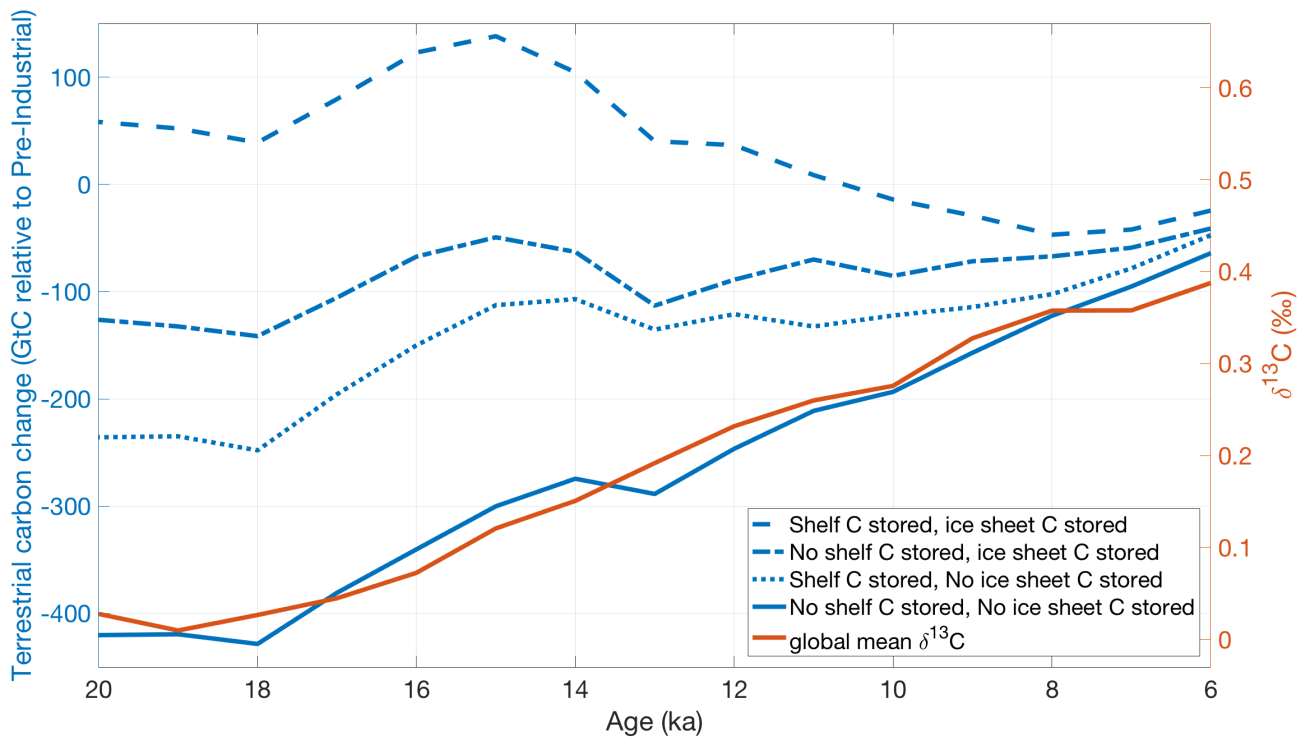


Figure 5. Time series of various Four HadCM3 simulations of terrestrial carbon storage change (biosphere and soils) anomalies relative to the pre-Industrial plotted in blue (blue, Davies-Barnard et al., 2017) and compared to our volume-weighted global mean benthic $\delta^{13}\text{C}$ approximation of terrestrial carbon storage plotted in stack (orange). Global mean $\delta^{13}\text{C}$ change most closely resembles one the simulation (solid blue) that releases carbon from under ice sheets to the atmosphere and does not store carbon on continental shelves (solid blue). The two y-axes are scaled to illustrate the similarity in the pattern of change across the deglaciation but are not meant to imply that the magnitude of change is equivalent.

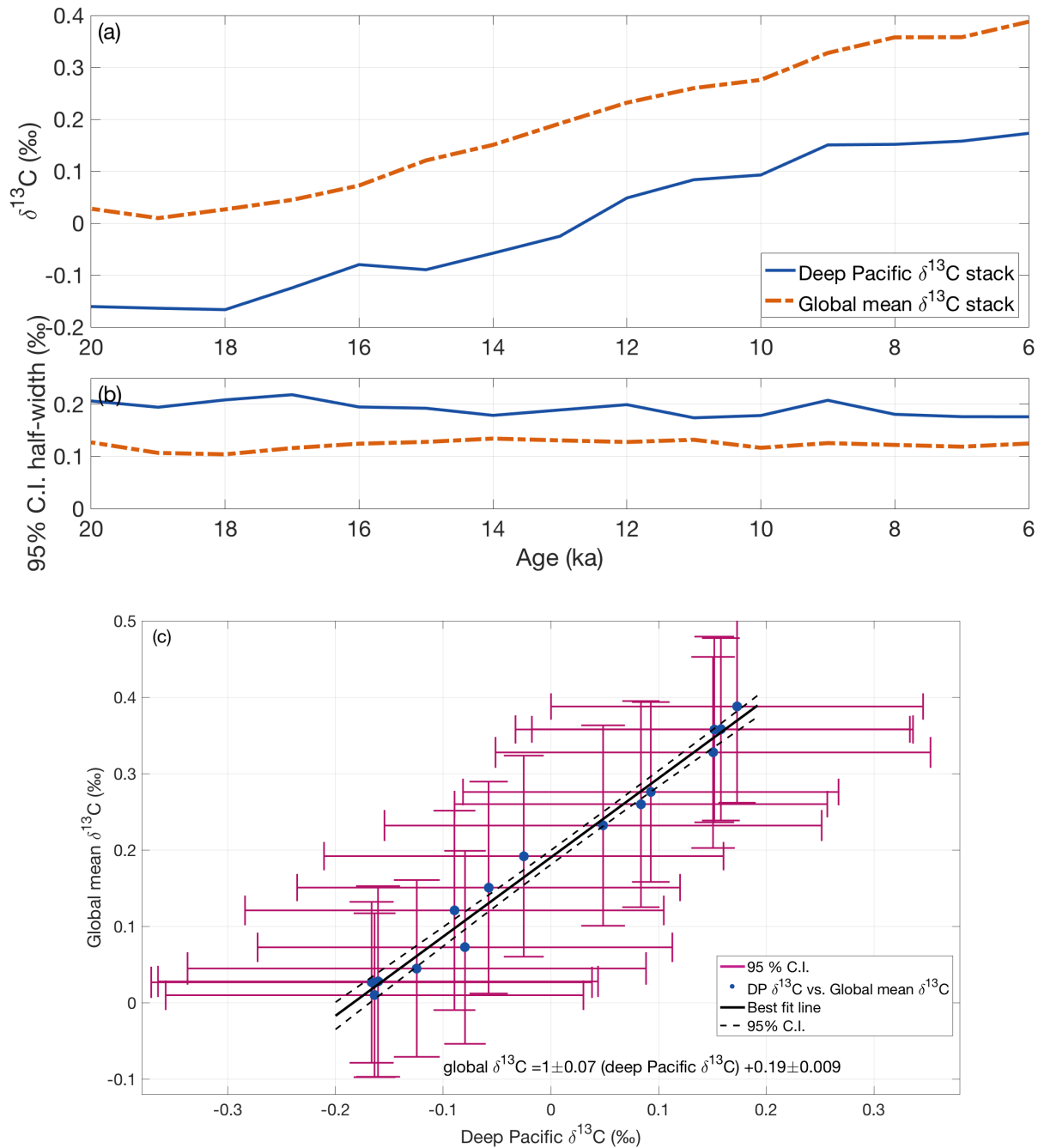


Figure 6. (a) Time series of global mean ocean $\delta^{13}\text{C}$ stack and deep Pacific $\delta^{13}\text{C}$ stacks. (b) Half-width 95% confidence intervals for the global mean stack and deep Pacific stack. (c) Deep Pacific $\delta^{13}\text{C}$ stack vs. global mean $\delta^{13}\text{C}$ stack. Each point is the $\delta^{13}\text{C}$ value for one time slice with 95% confidence intervals (vertical and horizontal error bars). Time across the deglaciation progresses toward the upper right corner. The best-fit [line for the two stacks](#) [linear regression](#) is plotted as a solid line with 95% confidence interval (dashed lines).

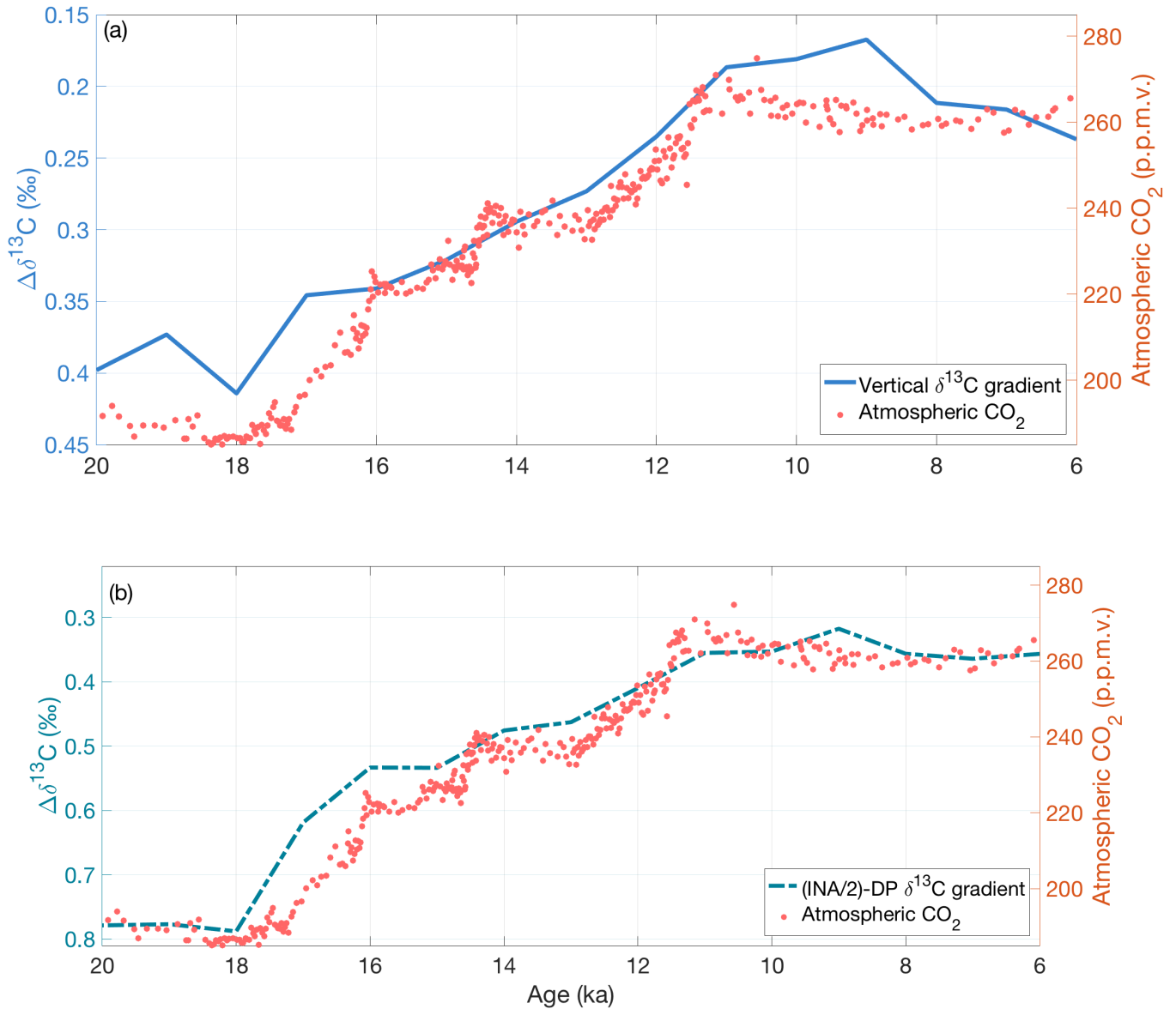


Figure 7. Comparison of atmospheric CO₂ with ~~both AP~~ (a) the vertical $\delta^{13}\text{C}$ gradient (~~excluding the data-sparse Indian regions~~) and $\Delta\delta^{13}\text{C}_{(INA/2)-DP}$ gradient (b) $\Delta\delta^{13}\text{C}_{(INA/2)-DP}$. Both ~~vertical~~ gradients ~~closely resemble the spliced~~ have a statistically significant correlation with atmospheric CO₂ records (red circles) (Marcott et al., 2014; Monnin et al., 2004), ~~but the $\Delta\delta^{13}\text{C}_{(INA/2)-DP}$ gradient is better correlated with atmospheric CO₂ from 20-6 ka?~~. Recall the ~~The~~ y-axes for (a) and (b) are scaled differently because $\Delta\delta^{13}\text{C}_{(INA/2)-DP}$ gradient is not volume-weighted ~~scales the intermediate North Atlantic stack by half before subtracting the deep Pacific stack~~ while the ~~vertical AP~~ $\delta^{13}\text{C}$ gradient is volume-weighted, hence the ~~right y-axes~~ difference between the ~~top~~ Atlantic-Pacific intermediate and ~~bottom~~ panels are not directly comparable ~~deep~~ stacks.

Table 1. Region details: number of sites included, the regional Regional stack information. The total volume as a percent of represented by the core depth range global stack of all nine regions (spanning 0.5-5 km -, and excluding shallow inland seas, Southern Ocean, and Arctic Ocean) -, and is 77.7% of the mean whole ocean. The volume of each region is listed as a percent of the global stack volume (rather than whole ocean volume). For each stack we list its $\delta^{13}\text{C}$ estimates value at the LGM (20 ka), Holocene (6 ka), and the Holocene $\delta^{13}\text{C}$ minus LGM $\delta^{13}\text{C}$ difference. In parenthesis are bootstrapped mean $\delta^{13}\text{C}$ values and The 95% confidence interval for the global mean $\delta^{13}\text{C}$ change is provided in parentheses. The full time series for each stack is provided in supplemental material.

Region name	Sites in stack	%Volume [*]	$\delta^{13}\text{C}_{Hol}(\text{‰})$	$\delta^{13}\text{C}_{LGM}(\text{‰})$	$\Delta\delta^{13}\text{C}_{Hol-LGM}(\text{‰})$
INA	18	5.0	1.06	1.24	-0.18
ISA	<u>9-14</u>	7.9	<u>0.96-1.0</u>	<u>0.59-0.65</u>	0.37
II	2	8.0	0.16	0.01	0.15
IP	6	24.3	0.31	-0.02	0.32
Intermediate <u>w, m AP</u>	35	45.2	<u>0.55-0.57_w</u>	<u>0.29-0.30_w</u>	0.26 _w
UDNA	49	5.4	0.92	0.44	0.48
LDNA	10	1.5	0.75	0.04	0.71
DSA	<u>14-19</u>	6.2	<u>0.42-0.55</u>	<u>-0.38-0.24</u>	<u>0.80-0.79</u>
DI	2	9.5	0.15	-0.46	0.61
DP	7	32.2	0.17	-0.16	0.33
Deep <u>w, m AP</u>	82	54.8	<u>0.31-0.33_w</u>	<u>-0.12-0.10_w</u>	<u>0.43-0.42_w</u>
Global <u>$w, +$ \pm</u>	<u>117-127</u>	77.7*	<u>0.37-0.39_w</u>	<u>0.01-0.03_w</u>	0.36 _w (95% CI: <u>0.25 to 0.46, 0.23 to 0.50</u>)

*Volume of core depth range (0.5-5 km)-all regions as a proportion of global whole-ocean volume

w Volume-weighted $\delta^{13}\text{C}$ values, m Excluding the Indian Ocean regions

w Volume-weighted $\delta^{13}\text{C}$ values

+Atlantic, Indian, and Pacific Ocean regions

Table 2. Correlation coefficients and p-values between pre-whitened records. ~~We pre-whitened to account for autocorrelated~~ Pre-whitening reduces the impact of autocorrelation in the time series ~~and calculated~~. Calculated p-values ~~to account for the~~ reduced degrees of freedom ~~for in~~ pre-whitened and ~~or time lagged~~ time-lagged correlations. ~~To investigate possible leads~~ Non-zero CO₂ time shifts indicate the lead/lags between records, we shift lag adjustment that maximizes the correlation between atmospheric CO₂ record in 100-year increments relative to ~~?~~ and the $\delta^{13}\text{C}$ stacks. The atmospheric CO₂ record is spliced from CO₂ records from Monnin et al. (2004) at 8.9855 ka and Marcott et al. (2014) at 8.9730 ka ~~stack or gradient~~.

Record 1	Record 2	CO ₂ time shift (years)	Pre-whitened r ²	Pre-whitened p-value
Global mean $\delta^{13}\text{C}$ stack	Deep Pacific $\delta^{13}\text{C}$ stack	0	0.46	0.05
CO ₂	Deep Pacific $\delta^{13}\text{C}$ stack	0	0.62 <u>0.57</u>	0.008 <u>0.02</u>
CO ₂	Global $\delta^{13}\text{C}$ stack	0	0.20 <u>0.28</u>	0.24 <u>0.16</u>
CO ₂	Global $\delta^{13}\text{C}$ stack	-500 <u>600</u>	0.35 <u>0.39</u>	0.12 <u>0.09</u>
CO ₂	$\Delta\delta^{13}\text{C}_{I-D}$	0	-0.70 <u>-0.51</u>	0.002 <u>0.03</u>
CO ₂	$\Delta\delta^{13}\text{C}_{I-D}$	+300 <u>-400</u>	-0.73 <u>-0.66</u>	0.002 <u>0.006</u>
CO ₂	$\Delta\delta^{13}\text{C}_{(INA/2)-DP}$	0	-0.79 <u>-0.69</u>	0.0002 <u>0.003</u>
CO ₂	$\Delta\delta^{13}\text{C}_{(INA/2)-DP}$	-200 <u>400</u>	-0.82 <u>-0.78</u>	0.0002 <u>0.0006</u>

Appendix A

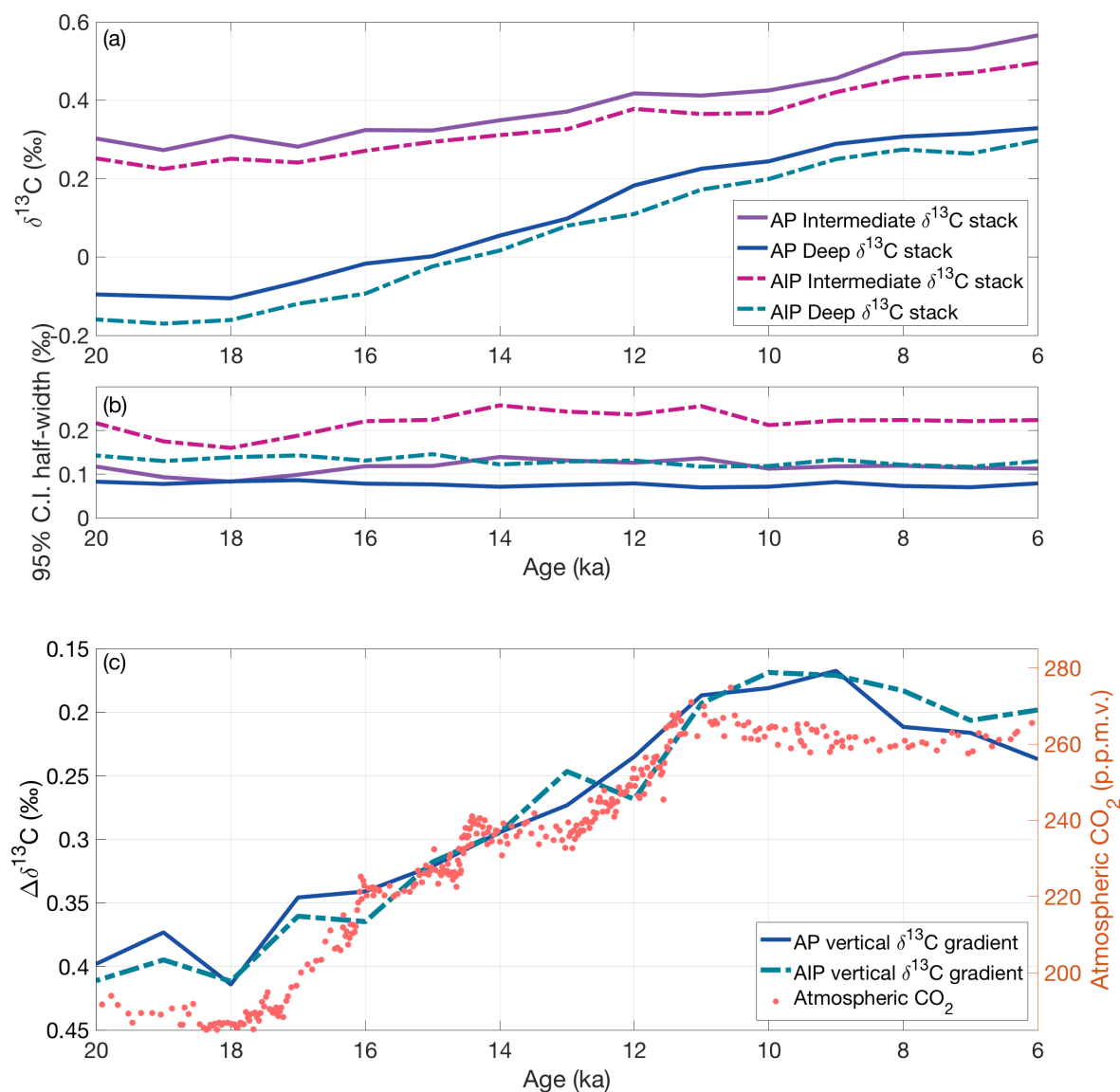


Figure A1. (Aa) Two versions of the deep and intermediate stacks with the AP stacks (solid lines) include only Atlantic and Pacific regions and AIP stacks plotted in (dot-dashed lines) include Atlantic, Indian, and AP stacks plotted in solid lines Pacific regions. (Bb) The 95% C.I. half-width for each stack in the legend in figure (A). (Cc) Comparison of CO_2 and both AP and AIP vertical $\delta^{13}\text{C}$ gradients. Both volume-weighted vertical gradients closely resemble the spliced atmospheric CO_2 records (red circles) (Marcott et al., 2014; Monnin et al., 2004) (?), but the AIP $\delta^{13}\text{C}$ gradient (dashed green-blue line) is more noisy and slightly more depleted less smooth than the AP $\delta^{13}\text{C}$ gradient (solid blue line) during the termination.

Table A1. Supplemental table of the name, location, region, and reference for each record in this compilation of $\delta^{13}\text{C}$ synthesis. Asterisks mark cores for which we use the cited authors' radiocarbon age model instead of using the regional age model from Stern and Lisiecki (2014).

Core name	Name	Lat Latitude	Lon Longitude	Depth (m)	Region	Reference	DOI
EW9209-1JPC		5.9-29.3	-44.2 -11.5	4056-796	LDNA INA	Curry and Oppo (1997) Sarnthein et al. (2003)	https://doi.org/10.1594/PANGAEA.54372
GIK16006-1							
GeoB7920-2		20.8-34.9	-18.6-7.1	2278-803	UDNA INA	Tjallingii et al. (2008) Sarnthein et al. (2003)	https://doi.org/10.1594/PANGAEA.54381
GIK15666-6							
GeoB9508-5		14.5-21.3	-17.9-17.8	2384-812	UDNA INA	Mulitz et al. (2008) Sarnthein et al. (2004)	https://doi.org/10.1594/PANGAEA.134784
GIK16017							
GeoB9526		12.4-52.2	-18.1	3223-900	UDNA INA	Zarriess and Mackensen (2011) Sarnthein et al. (2003)	https://doi.org/10.1594/PANGAEA.134554
GeoB6718			-12.8			et al (2005)	
GIK17049-6		55.3-26.1	-26.7	3331-965	UDNA INA	Jung and Sarnthein (2003) Caballero et al. (2008)	https://www.ncdc.noaa.gov/paleo/study/8720
OCE205-103GGC			-78.1				
GIK17051		56.2-57.5	-31.9	2295	UDNA INA	Sarnthein et al. (1994) Venz et al. (1999)	https://www.ncdc.noaa.gov/paleo/study/2550
ODP982			-15.9	1134			
GIK23415-9		53.2-12.1	-19.2	2472	UDNA INA	Weinelt et al. (2003) Huels et al. (2000)	https://doi.org/10.1594/PANGAEA.55754
M35003-4			-61.2	1299			
KF13		37.6-28.9	-31.8	2690	UDNA INA	Richter (1998) Freudenthal et al. (2003)	https://www.pangaea.de/10.1594/PANGAEA.57859
GeoB4240			-13.2	1358			
MD95-2040		40.6-54.9	-9.9-19.8	2465	UDNA INA	Voelker and de Abreu (2011) Sarnthein et al. (2003)	https://doi.org/10.1594/PANGAEA.112916
GIK23419				1491			
MD99-2334		37.8-21.2	-10.2	3146	UDNA INA	Skinner and Shackleton (2004) Sarnthein et al. (2003)	https://doi.org/10.1594/PANGAEA.54374
GIK16030			-18.1	1500			
NA87-22		55.5-29.9	-14.7	2161	UDNA INA	Duplessy et al. (1992) Sarnthein et al. (2003)	https://doi.org/10.1594/PANGAEA.54371
GIK16004			-10.7	1512			
ODP658C		20.8-61	-18.6-24	2274	UDNA INA	Woodruff and Chambers (1991) Sarnthein et al. (2003)	https://doi.org/10.1594/PANGAEA.54374
ODP984				1650			
ODP980		55.5-11.7	-14.7	2168	UDNA INA	Oppo et al. (2006) Oppo and Fairbanks (1987)	https://doi.org/10.1594/PANGAEA.52404
V28-127			-80.1	1750			
SU90-03		40.1-35.6	-32-8.1	2475	UDNA INA	Cortijo et al. (1999) Weinelt and Sarnthein (2003)	https://doi.org/10.1594/PANGAEA.97104
GIK11944-2				1765			
V29-202		61-11.5	-21-79.4	2658	UDNA INA	Oppo and Lehman (1995) DeConto et al. (2006)	https://www.ncdc.noaa.gov/paleo/study/2554
DSDP502				1800			
ENO66-16		5.5-64.8	-21.1	3152	UDNA INA	Oppo and Fairbanks (1987) Cortijo et al. (1998)	https://doi.org/10.1594/PANGAEA.726195
V28-14			-29.7	1855			
ENO66-21		4.2-64.8	-21.6	3995	UDNA INA	Oppo and Fairbanks (1987) Cortijo et al. (1998)	https://doi.org/10.1594/PANGAEA.271549
GIK23519			-29.6	1893			

Core name	Name	Lat Latitude	Lon Longitude	Depth (m)	Region	Reference	DOI
GIK23418-8		52.6	-20.3	2841	UDNA	Jung and Sarnthein (2004)	https://doi.org/10.1594/PANGAEA.54366
GIK12392-1			-16.9	2573			
IODP-U1308		49.9	-24.2	3900	UDNA	Hodell et al. (2008)	https://doi.org/10.1594/PANGAEA.54364
GIK12347-2			-17.9	2576			
KNR110-50		4.9	-43.2	3995	UDNA	Curry et al. (1988)	https://www.ncdc.noaa.gov/paleo/study/21450
V29-202				2658		Oppo and Lehman (1995)	
KNR110-55		4.9	-42.9	4556	LDNA	Curry et al. (1988)	https://doi.org/10.1594/PANGAEA.66317
KF13			-31.8	2690	UDNA	Richter (1998)	
KNR110-58		4.8	-43	4341	LDNA	Curry et al. (1988)	https://doi.org/10.1594/PANGAEA.52049
GIK12328-5		21.2	-18.6	2778	UDNA	Sarnthein et al. (1994)	
KNR110-66		4.6	-43.4	3547	UDNA	Curry et al. (1988)	https://www.ncdc.noaa.gov/paleo/study/2524
HM52-43		63.5	-0.7	2781		Fronval and Jansen (1997)	
KNR110-71		4.4	-43.7	3164	UDNA	Jung and Sarnthein (2003)	https://doi.org/10.1594/PANGAEA.112909
GIK17050			-27.9	2795			
KNR110-82		4.3	-43.5	2816	UDNA	Curry et al. (1988)	https://doi.org/10.1594/PANGAEA.357162
GIK23418-8		52.6	-20.3	2841	UDNA	Jung and Sarnthein (2003)	https://doi.org/10.1594/PANGAEA.112915
EN066-38		4.9	-20.5	2937	UDNA	Curry and Lohmann (1983)	https://doi.org/10.1594/PANGAEA.726019
GIK15612-2		44.4	-26.5	3050	UDNA	Sarnthein et al. (1994)	https://doi.org/10.1594/PANGAEA.54369
KNR110-75		4.3	-43.4	3063	UDNA	Curry et al. (1988)	https://doi.org/10.1594/PANGAEA.357161
KNR110-82		4.3	-43.5	2816	UDNA	Curry et al. (1988)	https://doi.org/10.1594/PANGAEA.52327
CHN82-24		43.5	-30.7	3070			
KNR110-91		4.8	-43.3	3810	UDNA	Curry et al. (1988)	https://doi.org/10.1029/PA003i003p00317
V30-49			-21.1	3093			
MD95-2039		40.6	-10.4	3381	UDNA	Schönfeld et al. (2003)	https://doi.org/10.1594/PANGAEA.738036
MD99-2334			-10.2	3146			
ODP928		5.5	-43.8	4012	LDNA	Curry and Oppo (2005)	https://doi.org/10.1594/PANGAEA.726013
EN066-16			-21.1	3160	UDNA	Curry and Lohmann (1983)	
SU90-39		52.5	-22	3955	UDNA	Chapman and Shackleton (1998)	https://doi.org/10.1594/PANGAEA.357160
KNR110-71		4.4	-43.7	3164			
V22-197		14.2	-18.6	3167	UDNA	Boyle (1992)	https://doi.org/10.1594/PANGAEA.52291
V23-81		54.3	-16.8	2393	UDNA	Yeum et al. (1992)	https://doi.org/10.1594/PANGAEA.756414

<u>Core name</u>	<u>-40.9</u> <u>Latitude</u>	<u>9.9</u> <u>Longitude</u>	<u>4621</u> <u>Depth</u> <u>(m)</u>	<u>DSA</u> <u>Region</u>	<u>Hodell et al. (2001)</u> <u>Reference</u> <u>DOI</u>
<u>ODP1090</u> <u>KNR110-55</u>	<u>4.9</u>	<u>-42.9</u>	<u>8.9</u> <u>4556</u>	<u>3702</u> <u>LDNA</u>	<u>DSA</u> <u>Curry et al. (1988)</u> <u>Venz and Hodell (2002)</u> https://doi.org/10.1594/PANGAEA.357157
<u>PS2498</u> <u>GeoB1101</u>	<u>-44.2</u> <u>-1.7</u>	<u>-14.2</u> <u>-10.9</u>	<u>3783</u> <u>4588</u>	<u>DSA</u> <u>LDNA</u>	<u>Hodell et al. (2003)</u> <u>Bickert and Wefer (1996)</u> https://doi.org/10.1594/PANGAEA.103621
<u>RC13-228</u> <u>EN066-26</u>	<u>-22.3</u> <u>-3.1</u>	<u>11.2</u> <u>-20</u>	<u>3204</u> <u>4745</u>	<u>DSA</u> <u>LDNA</u>	<u>Boyle (1992)</u> <u>Curry and Lohmann (1983)</u> https://doi.org/10.1594/PANGAEA.726015
<u>V29-135</u> <u>EN066-32</u>	<u>2.5</u>	<u>-19.7</u>	<u>8.88</u> <u>4998</u>	<u>2675</u> <u>LDNA</u>	<u>DSA</u> <u>Curry and Sarnthein et al. (1994)</u> https://doi.org/10.1594/PANGAEA.726017
<u>V30-40</u> <u>GeoB3104</u>	<u>0.2</u> <u>-3.7</u>	<u>-23.2</u> <u>-37.7</u>	<u>3706</u> <u>767</u>	<u>DSA</u> <u>ISA</u>	<u>Oppo and Fairbanks (1987)</u> <u>Amos et al. (1999)</u> https://doi.org/10.1594/PANGAEA.54790
<u>Core Name</u> <u>BT4</u>	<u>Lat</u> <u>-4</u>	<u>Lon</u> <u>-10</u>	<u>Depth</u> <u>(m)</u> <u>1000</u>	<u>Region</u> <u>ISA</u>	<u>Reference</u> <u>Curry et al. (1988)</u> https://doi.org/10.1594/PANGAEA.52328
<u>DSDP502</u> <u>KNR159-5-90GGC-27.35</u>	<u>11.5</u>	<u>-79.4</u> <u>-46.63</u>	<u>1800</u> <u>1105</u>	<u>INA</u> <u>ISA</u>	<u>Demoucal et al. (1992)</u> <u>Curry and Oppo (2005)</u> http://www.noaa.gov/paleo/study/19521
<u>GeoB6718</u> <u>KNR159-5-36GGC-27.27</u>	<u>52.2</u>	<u>-12.8</u> <u>-46.47</u>	<u>900</u> <u>1268</u>	<u>INA</u> <u>ISA</u>	<u>Rüggeberg et al. (2005)</u> <u>Curry and Oppo (2005)</u> http://www.noaa.gov/paleo/study/19521
<u>GHK15666-6</u> <u>RC16-119</u>	<u>34.9</u> <u>-27.7</u>	<u>-7.1</u> <u>-46.5</u>	<u>803</u> <u>1567</u>	<u>INA</u> <u>ISA</u>	<u>Sarnthein et al. (1994)</u> <u>Oppo (2005)</u> http://www.noaa.gov/paleo/study/2592
<u>GHK16006-1</u> <u>KNR159-5-17JPC</u>	<u>29.3</u> <u>-27.7</u>	<u>-11.5</u> <u>-46.49</u>	<u>796</u> <u>1627</u>	<u>INA</u> <u>ISA</u>	<u>Sarnthein et al. (1994)</u> <u>Tessin and Oppo (2005)</u> http://www.noaa.gov/paleo/study/19521
<u>GHK16017</u> <u>KNR159-5-78GGC-27.48</u>	<u>21.3</u>	<u>-17.8</u> <u>-46.33</u>	<u>812</u> <u>1829</u>	<u>INA</u> <u>ISA</u>	<u>Sarnthein et al. (1994)</u> <u>Tessin and Oppo (2005)</u> http://www.noaa.gov/paleo/study/19521
<u>OCE205-103GGC-27.42</u> <u>V24-25.9</u>	<u>24.2</u> <u>-25.9</u>	<u>-78.1</u> <u>-44.7</u>	<u>965</u> <u>2069</u>	<u>INA</u> <u>ISA</u>	<u>Slowey and Curry (1995)</u> <u>Oppo and Morawitz (2000)</u> http://www.noaa.gov/paleo/study/2592
<u>GeoB4240</u> <u>KNR159-5-33GGC-27.57</u>	<u>28.9</u>	<u>-13.2</u> <u>-46.18</u>	<u>1358</u> <u>2082</u>	<u>INA</u> <u>ISA</u>	<u>Freudenthal et al. (2002)</u> <u>Tessin and Oppo (2005)</u> http://www.noaa.gov/paleo/study/19521
<u>GHK11944-2</u> <u>ODP1088</u>	<u>35.6</u> <u>-41.1</u>	<u>-8.1</u> <u>-13.6</u>	<u>1765</u> <u>2082</u>	<u>INA</u> <u>ISA</u>	<u>Weinelt and Sarnthein (2003)</u> https://doi.org/10.1594/PANGAEA.218111
<u>GHK16004</u> <u>KNR159-5-42JPC</u>	<u>29.9</u> <u>-27.76</u>	<u>-10.7</u> <u>-46.63</u>	<u>1512</u> <u>2296</u>	<u>INA</u> <u>ISA</u>	<u>Sarnthein et al. (1994)</u> <u>Curry and Oppo (2005)</u> http://www.noaa.gov/paleo/study/19521
<u>GHK16030</u> <u>CHN115-70</u>	<u>21.2</u> <u>-29.9</u>	<u>-18.1</u> <u>-35.6</u>	<u>1500</u> <u>2340</u>	<u>INA</u> <u>ISA</u>	<u>Sarnthein et al. (1994)</u> <u>Curry and Lohmann (1982)</u> https://doi.org/10.1594/PANGAEA.726254
<u>GHK23419</u> <u>RC16-84</u>	<u>54.9</u> <u>-26.7</u>	<u>-19.8</u> <u>-43.3</u>	<u>1491</u> <u>2438</u>	<u>INA</u> <u>ISA</u>	<u>Sarnthein et al. (1994)</u> <u>Oppo (2005)</u> http://www.noaa.gov/paleo/study/2592

<u>Core name</u>	<u>14.6</u> <u>Latitude</u>	<u>52.9</u> <u>Longitude</u>	<u>1803</u> <u>Depth</u> <u>(m)</u>	<u>H</u> <u>Region</u>	<u>Schmiedl and Mackensen (2005)</u> <u>Reference</u>
MD01-2378	-13.1	121.8	1783	II	Xu et al. (2008) Holbourn et al. (2005) https://doi.org/10.1594/PANGAEA.263755
GeoB3004	14.6	52.9	1803	II	Schmiedl and Leuschner (2005) https://doi.org/10.1594/PANGAEA.315174
Orgon4-KS8	23.5	59.2	2900	DI	Sirocko (1994) Sirocko et al. (2002) https://doi.org/10.1594/PANGAEA.52392
SO42-74KL	14.3	57.3	3212	DI	Sirocko et al. (1993) Sirocko et al. (2002) https://doi.org/10.1594/PANGAEA.52389
MD97-2151 <u>FR97-GC12</u>	8.7-23.6 <u>153.8</u>	109.9 <u>153.8</u>	1598-990 <u>153.8</u>	IP	Wei et al. (2006) Bostock et al. (2004) https://doi.org/10.1594/PANGAEA.832096
FR97-GC12 <u>MD97-2120</u>	-23.6 <u>-45.5</u>	153.8 <u>174.9</u>	990-1210 <u>174.9</u>	IP	Bostock et al. (2004) Pahnke and Zahn (2005) https://doi.org/10.1594/PANGAEA.51844
V19-27	-0.5	-82.1	1373	IP	Mix et al. (1991) https://doi.org/10.1594/PANGAEA.51844
EW9504-05 <u>MD97-2151</u>	32.5-8.7 <u>109.9</u>	-118.1 <u>109.9</u>	1818 <u>1598</u>	IP	Stott et al. (2000) Chen (2003) https://doi.pangaea.de/10.1594/PANGAEA.114672
GIK17961-2	8.5	112.3	1795	IP	Wang et al. (1999) https://doi.org/10.1594/PANGAEA.54714
MD97-2120 <u>EW9504-05</u>	-45.5-32.5 <u>-118.1</u>	174.9 <u>-118.1</u>	1210 <u>1818</u>	IP	Pahnke and Zahn (2005) Stott et al. (2000) https://www.ncdc.noaa.gov/paleo/study/2546
Core Name <u>V24-109</u>	Lat-0.4 <u>158.8</u>	Lon-158.8 <u>2367</u>	Depth <u>(m)-2367</u>	Region <u>DP</u>	Reference <u>Shackleton et al. (1992)</u>
NGC102	32.3	157.9	2612	DP	Ohkushi et al. (2003) https://doi.org/10.1016/S0377-8398(03)00023-9
ODP807A <u>ODP1143</u>	3.6-9.4 <u>113.3</u>	156.6 <u>113.3</u>	2804 <u>2772</u>	DP	Zhang et al. (2007) Tian et al. (2002) https://doi.org/10.1594/PANGAEA.700904
ODP846 <u>ODP807A</u>	-3.1-3.6 <u>156.6</u>	-90.8 <u>156.6</u>	3296 <u>2804</u>	DP	Mix et al. (1995); Shackleton et al. (1995) Zhan et al. (2007) http://www.ncdc.noaa.gov/paleo/study/2007.03.003
RC13-110	-0.1	-95.7	3231	DP	Mix et al. (1991) Marchitto et al. (2005) https://www.ncdc.noaa.gov/paleo/study/2511
V24-109 <u>ODP846</u>	0.4-3.1 <u>-90.8</u>	158.8 <u>-90.8</u>	2367 <u>3296</u>	DP	Shackleton et al. (1992) Mix et al. (1995) https://www.ncdc.noaa.gov/paleo/study/2533
ODP1143 <u>RC13-114</u>	9.4-1.7 <u>-103.6</u>	113.3 <u>-103.6</u>	2772 <u>3436</u>	DP	Tian et al. (2002) Marchitto et al. (2005) https://doi.org/10.1594/PANGAEA.712938

Table A2. Correlation coefficients and p-values between records. The upper rows ~~are use~~ the raw data, and the bottom rows ~~are the use~~ pre-whitened data to account for autocorrelated time series. AIP gradients include Atlantic, Indian and Pacific regions, and AP graients include only Atlantic and Pacific regions. To investigate possible leads/lags between records, we shift the atmospheric CO₂ record in 100-year increments relative to the $\delta^{13}\text{C}$ stacks and, for brevity, list only the best correlations. All p-values account for reduction in degrees of freedom due to ~~either~~ pre-whitening and/or time shifting.

Record 1	Record 2	CO ₂ time shift (years)	r ²	
CO ₂	API AIP $\Delta\delta^{13}\text{C}_{I-D}$	0	-0.97 <u>-0.96</u>	
CO ₂	API AIP $\Delta\delta^{13}\text{C}_{I-D}$	+1000 <u>-700</u>	-0.99	
CO ₂	AP $\Delta\delta^{13}\text{C}_{I-D}$	0	-0.98 <u>-0.96</u>	
CO ₂	AP $\Delta\delta^{13}\text{C}_{I-D}$	+600 <u>-100</u>	-0.98 <u>-0.97</u>	
CO ₂	$\Delta\delta^{13}\text{C}_{(INA/2)-DP}$	0	-0.98	
CO ₂	$\Delta\delta^{13}\text{C}_{(INA/2)-DP}$	-200 <u>400</u>	-0.98 <u>-0.99</u>	
CO ₂	Global $\delta^{13}\text{C}$ stack	0	0.93 <u>0.94</u>	
CO ₂	Global $\delta^{13}\text{C}$ stack	+1000 <u>800</u>	0.95 <u>0.97</u>	
Record 1	Record 2	CO ₂ time shift (years)	Pre-whitened r ²	Pre-whitened p-value
CO ₂	API AIP $\Delta\delta^{13}\text{C}_{I-D}$	0	-0.39 <u>-0.25</u>	0.08 <u>0.19</u>
CO ₂	API AIP $\Delta\delta^{13}\text{C}_{I-D}$	+900 <u>800</u>	-0.80 <u>-0.62</u>	0.0003 <u>0.01</u>
CO ₂	AP $\Delta\delta^{13}\text{C}_{I-D}$	0	-0.70 <u>-0.50</u>	0.002 <u>0.03</u>
CO ₂	AP $\Delta\delta^{13}\text{C}_{I-D}$	+300 <u>-400</u>	-0.73 <u>-0.65</u>	0.002 <u>0.007</u>
CO ₂	$\Delta\delta^{13}\text{C}_{(INA/2)-DP}$	0	-0.79 <u>-0.69</u>	0.0002 <u>0.003</u>
CO ₂	$\Delta\delta^{13}\text{C}_{(INA/2)-DP}$	-200 <u>+400</u>	-0.82 <u>-0.78</u>	0.0002 <u>0.001</u>
CO ₂	Global $\delta^{13}\text{C}$ stack	0	0.20 <u>0.29</u>	0.24 <u>0.16</u>
CO ₂	Global $\delta^{13}\text{C}$ stack	-500	0.36 <u>0.37</u>	0.11 <u>0.10</u>

Competing interests. The authors declare that they have no conflict of interest.

Acknowledgements. We acknowledge the following colleagues [and reviewers](#) whose advice and input substantially improved drafts of this manuscript: David Lea, Syee Weldeab, Jake Gebbie, Andy Ridgwell, ~~and James Rae~~ [James Rae](#), [Andreas Schmittner](#), [Peter Köhler](#), and an [anonymous reviewer](#). Funding for this work came from NSF grants MGG 0926735 and CDI 1125181.

References

- Allen, K. A., Sikes, E. L., Hönisch, B., Elmore, A. C., Guilderson, T. P., Rosenthal, Y., and Anderson, R. F.: Southwest Pacific deep water carbonate chemistry linked to high southern latitude climate and atmospheric CO₂ during the last glacial termination, *Quaternary Science Reviews*, 122, 180–191, 2015.
- Archer, D., Winguth, A., Lea, D., and Mahowald, N.: What caused the glacial/interglacial atmospheric pCO₂ cycles?, *Reviews of Geophysics* - Richmond Virginia, then Washington, 38, 159–190, 2000.
- Archer, D. E., Martin, P. A., Milovich, J., Brovkin, V., Plattner, G.-K., and Ashendel, C.: Model sensitivity in the effect of Antarctic sea ice and stratification on atmospheric pCO₂, *Paleoceanography*, 18, 2003.
- Arz, H. W., Pätzold, J., and Wefer, G.: The deglacial history of the western tropical Atlantic as inferred from high resolution stable isotope records off northeastern Brazil, *Earth and Planetary Science Letters*, 167, 105–117, 1999.
- Aydin, M., Campbell, J., Fudge, T., Cuffey, K., Nicewonger, M., Verhulst, K., and Saltzman, E.: Changes in atmospheric carbonyl sulfide over the last 54,000 years inferred from measurements in Antarctic ice cores, *Journal of Geophysical Research: Atmospheres*, 2016.
- Bauska, T. K., Baggenstos, D., Brook, E. J., Mix, A. C., Marcott, S. A., Petrenko, V. V., Schaefer, H., Severinghaus, J. P., and Lee, J. E.: Carbon isotopes characterize rapid changes in atmospheric carbon dioxide during the last deglaciation, *Proceedings of the National Academy of Sciences*, 113, 3465–3470, 2016.
- Bertram, C. J., Elderfield, H., Shackleton, N. J., and MacDonald, J. A.: Cadmium/calcium and carbon isotope reconstructions of the glacial northeast Atlantic Ocean, *Paleoceanography*, 10, 563–578, 1995.
- Bickert, T. and Mackensen, A.: Last Glacial to Holocene changes in South Atlantic deep water circulation, in: *The South Atlantic in the Late Quaternary*, pp. 671–693, Springer, 2003.
- Bickert, T. and Wefer, G.: Late Quaternary deep water circulation in the South Atlantic: Reconstruction from carbonate dissolution and benthic stable isotopes, in: *The South Atlantic*, pp. 599–620, Springer, 1996.
- Bickert, T. and Wefer, G.: South Atlantic and benthic foraminifer $\delta^{13}\text{C}$ deviations: implications for reconstructing the Late Quaternary deep-water circulation, *Deep Sea Research Part II: Topical Studies in Oceanography*, 46, 437–452, 1999.
- Bostock, H. C., Opdyke, B. N., Gagan, M. K., and Fifield, L. K.: Carbon isotope evidence for changes in Antarctic Intermediate Water circulation and ocean ventilation in the southwest Pacific during the last deglaciation, *Paleoceanography*, 19, 2004.
- Boyle, E. and Keigwin, L.: Comparison of Atlantic and Pacific paleochemical records for the last 215,000 years: Changes in deep ocean circulation and chemical inventories, *Earth and Planetary Science Letters*, 76, 135–150, 1985.
- Boyle, E. A.: Cadmium and delta ¹³C paleochemical ocean distributions during the stage 2 Glacial Maximum, *Annual Review of Earth and Planetary Sciences*, 20, 245, 1992.
- Broecker, W. S.: Ocean chemistry during glacial time, *Geochimica et Cosmochimica Acta*, 46, 1689–1705, 1982.
- Brovkin, V., Ganopolski, A., Archer, D., and Rahmstorf, S.: Lowering of glacial atmospheric CO₂ in response to changes in oceanic circulation and marine biogeochemistry, *Paleoceanography*, 22, 2007.
- Brovkin, V., Ganopolski, A., Archer, D., and Munhoven, G.: Glacial CO₂ cycle as a succession of key physical and biogeochemical processes, *Climate of the Past*, 8, 251–264, 2012.
- Buchanan, P. J., Matear, R. J., Lenton, A., Phipps, S. J., Chase, Z., and Etheridge, D. M.: The simulated climate of the Last Glacial Maximum and insights into the global marine carbon cycle, *Climate of the Past*, 12, 2271, 2016.
- Burke, A. and Robinson, L. F.: The Southern Ocean's role in carbon exchange during the last deglaciation, *Science*, 335, 557–561, 2012.

- Chapman, M. R. and Shackleton, N. J.: Millennial-scale fluctuations in North Atlantic heat flux during the last 150,000 years, *Earth and Planetary Science Letters*, 159, 57–70, 1998.
- Ciais, P., Tagliabue, A., Cuntz, M., Bopp, L., Scholze, M., Hoffmann, G., Laurantou, A., Harrison, S. P., Prentice, I., Kelley, D., et al.: Large inert carbon pool in the terrestrial biosphere during the Last Glacial Maximum, *Nature Geoscience*, 5, 74–79, 2012.
- Cortijo, E., Lehman, S., Keigwin, L., Chapman, M., Paillard, D., and Labeyrie, L.: Changes in meridional temperature and salinity gradients in the North Atlantic Ocean (30–72 N) during the last interglacial period, *Paleoceanography*, 14, 23–33, 1999.
- Crosta, X. and Shemesh, A.: Reconciling down core anticorrelation of diatom carbon and nitrogen isotopic ratios from the Southern Ocean, *Paleoceanography*, 17, 2002.
- Curry, W. and Lohmann, G.: Carbon isotopic changes in benthic foraminifera from the western South Atlantic: Reconstruction of glacial abyssal circulation patterns, *Quaternary Research*, 18, 218–235, 1982.
- Curry, W. B. and Oppo, D. W.: Synchronous, high-frequency oscillations in tropical sea surface temperatures and North Atlantic Deep Water production during the last glacial cycle, *Paleoceanography*, 12, 1–14, 1997.
- Curry, W. B. and Oppo, D. W.: Glacial water mass geometry and the distribution of $\delta^{13}\text{C}$ of ΣCO_2 in the western Atlantic Ocean, *Paleoceanography*, 20, 2005.
- Curry, W. B., Duplessy, J.-C., Labeyrie, L., and Shackleton, N. J.: Changes in the distribution of $\delta^{13}\text{C}$ of deep water ΣCO_2 between the last glaciation and the Holocene, *Paleoceanography*, 3, 317–341, 1988.
- Davies-Barnard, T., Ridgwell, A., Singarayer, J., and Valdes, P.: Quantifying the Influence of the Terrestrial Biosphere on Glacial-interglacial Climate Dynamics, *Climate of the Past*, 13, 1381–1401, 2017.
- Demenocal, P. B., Oppo, D. W., Fairbanks, R. G., and Prell, W. L.: Pleistocene $\delta^{13}\text{C}$ variability of North Atlantic intermediate water, *Paleoceanography*, 7, 229–250, 1992.
- Duplessy, J., Shackleton, N., Fairbanks, R., Labeyrie, L., Oppo, D., and Kallel, N.: Deepwater source variations during the last climatic cycle and their impact on the global deepwater circulation, *Paleoceanography*, 3, 343–360, 1988.
- Duplessy, J.-C., Labeyrie, L., Arnold, M., Paterne, M., Duprat, J., and van Weering, T. C.: Changes in surface salinity of the North Atlantic Ocean during the last deglaciation, *Nature*, 358, 485, 1992.
- Eggleston, S., Schmitt, J., Bereiter, B., Schneider, R., and Fischer, H.: Evolution of the stable carbon isotope composition of atmospheric CO_2 over the last glacial cycle, *Paleoceanography*, 2016.
- Ferrari, R., Jansen, M. F., Adkins, J. F., Burke, A., Stewart, A. L., and Thompson, A. F.: Antarctic sea ice control on ocean circulation in present and glacial climates, *Proceedings of the National Academy of Sciences*, 111, 8753–8758, 2014.
- Flower, B. P., Oppo, D. W., McManus, J., Venz, K., Hodell, D., and Cullen, J.: North Atlantic intermediate to deep water circulation and chemical stratification during the past 1 Myr, *Paleoceanography*, 15, 388, 2000.
- Franois, R., Altabet, M. A., Yu, E.-F., Sigman, D. M., Bacon, M. P., Frank, M., Bohrmann, G., Bareille, G., and Labeyrie, L. D.: Contribution of Southern Ocean surface-water stratification to low atmospheric CO_2 concentrations during the last glacial period, *Nature*, 389, 929–935, 1997.
- Freudenthal, T., Meggers, H., Henderiks, J., Kuhlmann, H., Moreno, A., and Wefer, G.: Upwelling intensity and filament activity off Morocco during the last 250,000 years, *Deep Sea Research Part II: Topical Studies in Oceanography*, 49, 3655–3674, 2002.
- Galbraith, E. D. and Jaccard, S. L.: Deglacial weakening of the oceanic soft tissue pump: global constraints from sedimentary nitrogen isotopes and oxygenation proxies, *Quaternary Science Reviews*, 109, 38–48, 2015.

- Gebbie, G., Peterson, C. D., Lisiecki, L. E., and Spero, H. J.: Global-mean marine $\delta^{13}\text{C}$ and its uncertainty in a glacial state estimate, *Quaternary Science Reviews*, 125, 144–159, 2015.
- Gildor, H., Tziperman, E., and Toggweiler, J.: Sea ice switch mechanism and glacial-interglacial CO_2 variations, *Global Biogeochemical Cycles*, 16, 2002.
- Gloege, L., McKinley, G. A., Mouw, C. B., and Ciochetto, A. B.: Global evaluation of particulate organic carbon flux parameterizations and implications for atmospheric pCO_2 , *Global Biogeochemical Cycles*, 31, 1192–1215, 2017.
- Gottschalk, J., Vázquez Riveiros, N., Waelbroeck, C., Skinner, L. C., Michel, E., Duplessy, J.-C., Hodell, D., and Mackensen, A.: Carbon isotope offsets between benthic foraminifer species of the genus *Cibicides* (*Cibicoides*) in the glacial sub-Antarctic Atlantic, *Paleoceanography*, 31, 1583–1602, 2016.
- Gu, S., Liu, Z., Zhang, J., Rempfer, J., Joos, F., and Oppo, D. W.: Coherent response of Antarctic Intermediate Water and Atlantic Meridional Overturning Circulation during the last deglaciation: reconciling contrasting neodymium isotope reconstructions from the tropical Atlantic, *Paleoceanography*, 32, 1036–1053, 2017.
- Herguera, J., Herbert, T., Kashgarian, M., and Charles, C.: Intermediate and deep water mass distribution in the Pacific during the Last Glacial Maximum inferred from oxygen and carbon stable isotopes, *Quaternary Science Reviews*, 29, 1228–1245, 2010.
- Hertzberg, J. E., Lund, D. C., Schmittner, A., and Skrivaneck, A. L.: Evidence for a biological pump driver of atmospheric CO_2 rise during Heinrich Stadial 1, *Geophysical Research Letters*, 43, 2016.
- Hesse, T., Butzin, M., Bickert, T., and Lohmann, G.: A model-data comparison of $\delta^{13}\text{C}$ in the glacial Atlantic Ocean, *Paleoceanography*, 26, 2011.
- Hodell, D. A., Kanfoush, S. L., Shemesh, A., Crosta, X., Charles, C. D., and Guilderson, T. P.: Abrupt cooling of Antarctic surface waters and sea ice expansion in the South Atlantic sector of the Southern Ocean at 5000 cal yr BP, *Quaternary Research*, 56, 191–198, 2001.
- Hodell, D. A., Venz, K. A., Charles, C. D., and Ninnemann, U. S.: Pleistocene vertical carbon isotope and carbonate gradients in the South Atlantic sector of the Southern Ocean, *Geochemistry, Geophysics, Geosystems*, 4, 1–19, 2003.
- Hodell, D. A., Channell, J. E., Curtis, J. H., Romero, O. E., and Röhl, U.: Onset of “Hudson Strait” Heinrich events in the eastern North Atlantic at the end of the middle Pleistocene transition (640 ka)?, *Paleoceanography*, 23, 2008.
- Hodell, D. A., Evans, H. F., Channell, J. E., and Curtis, J. H.: Phase relationships of North Atlantic ice-rafted debris and surface-deep climate proxies during the last glacial period, *Quaternary Science Reviews*, 29, 3875–3886, 2010.
- Hoffman, J. and Lund, D.: Refining the stable isotope budget for Antarctic Bottom Water: New foraminiferal data from the abyssal southwest Atlantic, *Paleoceanography*, 27, 2012.
- Hoogakker, B., Smith, R., Singarayer, J., Marchant, R., Prentice, I., Allen, J., Anderson, R., Bhagwat, S., Behling, H., Borisova, O., et al.: Terrestrial biosphere changes over the last 120 kyr, *Climate of the Past*, 12, 51–73, 2016.
- Joos, F., Gerber, S., Prentice, I., Otto-Bliesner, B. L., and Valdes, P. J.: Transient simulations of Holocene atmospheric carbon dioxide and terrestrial carbon since the Last Glacial Maximum, *Global Biogeochemical Cycles*, 18, 2004.
- Jung, S. and Sarnthein, M.: Stable isotope data of sediment cores GIK23415-9, PANGAEA, doi, 10, 2003.
- Jung, S. and Sarnthein, M.: Stable isotope analysis of foraminifera from sediment cores GIK17049-6, PANGAEA, doi, 10, 2004.
- Kallel, N., Labeyrie, L. D., Juillet-Leclerc, A., and Duplessy, J.-C.: A deep hydrological front between intermediate and deep-water masses in the glacial Indian Ocean, *Nature*, 333, 651–655, 1988.
- Kaplan, J. O., Prentice, I. C., Knorr, W., and Valdes, P. J.: Modeling the dynamics of terrestrial carbon storage since the Last Glacial Maximum, *Geophysical Research Letters*, 29, 2002.

- Kerr, J., Rickaby, R., Yu, J., Elderfield, H., and Sadekov, A. Y.: The effect of ocean alkalinity and carbon transfer on deep-sea carbonate ion concentration during the past five glacial cycles, *Earth and Planetary Science Letters*, 471, 42–53, 2017.
- Kohfeld, K. E. and Chase, Z.: Temporal evolution of mechanisms controlling ocean carbon uptake during the last glacial cycle, *Earth and Planetary Science Letters*, 472, 206–215, 2017.
- Kohfeld, K. E. and Ridgwell, A.: Glacial-interglacial variability in atmospheric CO₂, *Surface Ocean/Lower Atmosphere Processes, Geophysical Monograph Series*, 37, 2009.
- Köhler, P. and Fischer, H.: Simulating changes in the terrestrial biosphere during the last glacial/interglacial transition, *Global and Planetary Change*, 43, 33–55, 2004.
- Köhler, P., Joos, F., Gerber, S., and Knutti, R.: Simulated changes in vegetation distribution, land carbon storage, and atmospheric CO₂ in response to a collapse of the North Atlantic thermohaline circulation, *Climate Dynamics*, 25, 689–708, 2005.
- Köhler, P., Fischer, H., and Schmitt, J.: Atmospheric $\delta^{13}\text{C}_{\text{CO}_2}$ and its relation to pCO₂ and deep ocean $\delta^{13}\text{C}$ during the late Pleistocene, *Paleoceanography*, 25, 2010.
- Lacerra, M., Lund, D., Yu, J., and Schmittner, A.: Carbon storage in the mid-depth Atlantic during millennial-scale climate events, *Paleoceanography*, 2017.
- Landais, A., Lathiere, J., Barkan, E., and Luz, B.: Reconsidering the change in global biosphere productivity between the Last Glacial Maximum and present day from the triple oxygen isotopic composition of air trapped in ice cores, *Global biogeochemical cycles*, 21, 2007.
- Lisiecki, L.: Atlantic overturning responses to obliquity and precession over the last 3 Myr, *Paleoceanography*, 29, 71–86, 2014.
- Lisiecki, L. E.: A benthic $\delta^{13}\text{C}$ -based proxy for atmospheric pCO₂ over the last 1.5 Myr, *Geophysical Research Letters*, 37, n/a–n/a, <https://doi.org/10.1029/2010GL045109>, <http://dx.doi.org/10.1029/2010GL045109>, 121708, 2010.
- Lisiecki, L. E., Raymo, M. E., and Curry, W. B.: Atlantic overturning responses to Late Pleistocene climate forcings, *Nature*, 456, 85–88, 2008.
- Lund, D., Adkins, J., and Ferrari, R.: Abyssal Atlantic circulation during the Last Glacial Maximum: Constraining the ratio between transport and vertical mixing, *Paleoceanography*, 26, 2011a.
- Lund, D., Tessin, A., Hoffman, J., and Schmittner, A.: Southwest Atlantic water mass evolution during the last deglaciation, *Paleoceanography*, 30, 477–494, 2015.
- Lund, D. C., Mix, A. C., and Southon, J.: Increased ventilation age of the deep northeast Pacific Ocean during the last deglaciation, *Nature Geoscience*, 4, 771–774, 2011b.
- Lutze, G. and Thiel, H.: Epibenthic foraminifera from elevated microhabitats; *Cibicidoides wuellerstorfi* and *Planulina ariminensis*, *Journal of Foraminiferal Research*, 19, 153–158, 1989.
- Lynch-Stieglitz, J., Stocker, T. F., Broecker, W. S., and Fairbanks, R. G.: The influence of air-sea exchange on the isotopic composition of oceanic carbon: Observations and modeling, *Global Biogeochemical Cycles*, 9, 653–665, 1995.
- Lynch-Stieglitz, J., Adkins, J. F., Curry, W. B., Dokken, T., Hall, I. R., Herguera, J. C., Hirschi, J. J.-M., Ivanova, E. V., Kissel, C., Marchal, O., et al.: Atlantic meridional overturning circulation during the Last Glacial Maximum, *science*, 316, 66–69, 2007.
- Mackensen, A.: On the use of benthic foraminiferal $\delta^{13}\text{C}$ in palaeoceanography: constraints from primary proxy relationships, *Geological Society, London, Special Publications*, 303, 121–133, 2008.
- Mackensen, A. and Bickert, T.: Stable carbon isotopes in benthic foraminifera: proxies for deep and bottom water circulation and new production, in: *Use of proxies in paleoceanography*, pp. 229–254, Springer, 1999.

- Marchitto, T. M. and Broecker, W. S.: Deep water mass geometry in the glacial Atlantic Ocean: A review of constraints from the paleonutrient proxy Cd/Ca, *Geochemistry, Geophysics, Geosystems*, 7, 2006.
- Marchitto, T. M., Lynch-Stieglitz, J., and Hemming, S. R.: Deep Pacific CaCO₃ compensation and glacial–interglacial atmospheric CO₂, *Earth and Planetary Science Letters*, 231, 317–336, 2005.
- Marcott, S. A., Bauska, T. K., Buizert, C., Steig, E. J., Rosen, J. L., Cuffey, K. M., Fudge, T., Severinghaus, J. P., Ahn, J., Kalk, M. L., et al.: Centennial-scale changes in the global carbon cycle during the last deglaciation, *Nature*, 514, 616–619, 2014.
- Marinov, I., Follows, M., Gnanadesikan, A., Sarmiento, J. L., and Slater, R. D.: How does ocean biology affect atmospheric pCO₂? Theory and models, *Journal of Geophysical Research: Oceans*, 113, 2008a.
- Marinov, I., Gnanadesikan, A., Sarmiento, J. L., Toggweiler, J., Follows, M., and Mignone, B.: Impact of oceanic circulation on biological carbon storage in the ocean and atmospheric pCO₂, *Global Biogeochemical Cycles*, 22, 2008b.
- Martin, P. A. and Lea, D. W.: Comparison of water mass changes in the deep tropical Atlantic derived from Cd/Ca and carbon isotope records: Implications for changing Ba composition of deep Atlantic water masses, *Paleoceanography*, 13, 572–585, 1998.
- Martínez-García, A., Rosell-Melé, A., Geibert, W., Gersonde, R., Masqué, P., Gaspari, V., and Barbante, C.: Links between iron supply, marine productivity, sea surface temperature, and CO₂ over the last 1.1 Ma, *Paleoceanography*, 24, 2009.
- Martínez-Méndez, G., Zahn, R., Hall, I. R., Pena, L. D., and Cacho, I.: 345,000-year-long multi-proxy records off South Africa document variable contributions of Northern versus Southern Component Water to the Deep South Atlantic, *Earth and Planetary Science Letters*, 267, 309–321, 2008.
- Matsumoto, K. and Lynch-Stieglitz, J.: Similar glacial and Holocene deep water circulation inferred from southeast Pacific benthic foraminiferal carbon isotope composition, *Paleoceanography*, 14, 149–163, 1999.
- Matsumoto, K., Oba, T., Lynch-Stieglitz, J., and Yamamoto, H.: Interior hydrography and circulation of the glacial Pacific Ocean, *Quaternary Science Reviews*, 21, 1693–1704, 2002.
- Mc Intyre, K., Ravelo, A., and Delaney, M.: North Atlantic intermediate waters in the late Pliocene to early Pleistocene, *Paleoceanography*, 14, 324–335, 1999.
- McManus, J., Francois, R., Gherardi, J.-M., Keigwin, L., and Brown-Leger, S.: Collapse and rapid resumption of Atlantic meridional circulation linked to deglacial climate changes, *Nature*, 428, 834–837, 2004.
- Menviel, L., Joos, F., and Ritz, S.: Simulating atmospheric CO₂, $\delta^{13}C$ and the marine carbon cycle during the Last Glacial–Interglacial cycle: possible role for a deepening of the mean remineralization depth and an increase in the oceanic nutrient inventory, *Quaternary Science Reviews*, 56, 46–68, 2012.
- Menviel, L., Yu, J., Joos, F., Mouchet, A., Meissner, K., and England, M.: Poorly ventilated deep ocean at the Last Glacial Maximum inferred from carbon isotopes: A data-model comparison study, *Paleoceanography*, 32, 2–17, 2017.
- Millo, C., Sarnthein, M., Voelker, A., and Erlenkeuser, H.: Variability of the Denmark Strait overflow during the last glacial maximum, *Boreas*, 35, 50–60, 2006.
- Mix, A., Pisias, N., Zahn, R., Rugh, W., Lopez, C., and Nelson, K.: Carbon 13 in Pacific Deep and Intermediate Waters, 0-370 ka: Implications for Ocean Circulation and Pleistocene CO₂, *Paleoceanography*, 6, 205–226, 1991.
- Mix, A. C., Pisias, N. G., Rugh, W., Wilson, J., Morey, A., and Hagelberg, T.: Benthic foraminifer stable isotope record from Site 849 (0-5 Ma): Local and global climate changes, *Proceedings of the Ocean Drilling Program, Scientific Results*, 1995.

- Monnin, E., Steig, E. J., Siegenthaler, U., Kawamura, K., Schwander, J., Stauffer, B., Stocker, T. F., Morse, D. L., Barnola, J.-M., Bellier, B., et al.: Evidence for substantial accumulation rate variability in Antarctica during the Holocene, through synchronization of CO₂ in the Taylor Dome, Dome C and DML ice cores, *Earth and Planetary Science Letters*, 224, 45–54, 2004.
- Mulitza, S., Prange, M., Stuut, J.-B., Zabel, M., von Dobeneck, T., Itambi, A. C., Nizou, J., Schulz, M., and Wefer, G.: Sahel megadroughts triggered by glacial slowdowns of Atlantic meridional overturning, *Paleoceanography*, 23, 2008.
- Ohkushi, K., Itaki, T., and Nemoto, N.: Last Glacial–Holocene change in intermediate-water ventilation in the Northwestern Pacific, *Quaternary Science Reviews*, 22, 1477–1484, 2003.
- Oliver, K. I., Hoogakker, B. A., Crowhurst, S., Henderson, G., Rickaby, R., Edwards, N., and Elderfield, H.: A synthesis of marine sediment core $\delta^{13}\text{C}$ data over the last 150 000 years, *Climate of the Past*, 6, 645–673, 2010.
- Oppo, D. and Fairbanks, R.: Atlantic Ocean thermohaline circulation of the last 150,000 years: Relationship to climate and atmospheric CO₂, *Paleoceanography*, 5, 277–288, 1990.
- Oppo, D. W. and Fairbanks, R. G.: Variability in the deep and intermediate water circulation of the Atlantic Ocean during the past 25,000 years: Northern Hemisphere modulation of the Southern Ocean, *Earth and Planetary Science Letters*, 86, 1–15, 1987.
- Oppo, D. W. and Fairbanks, R. G.: Carbon isotope composition of tropical surface water during the past 22,000 years, *Paleoceanography*, 4, 333–351, 1989.
- Oppo, D. W. and Horowitz, M.: Glacial deep water geometry: South Atlantic benthic foraminiferal Cd/Ca and $\delta^{13}\text{C}$ evidence, *Paleoceanography*, 15, 147–160, 2000.
- Oppo, D. W. and Lehman, S. J.: Suborbital timescale variability of North Atlantic Deep Water during the past 200,000 years, *Paleoceanography*, 10, 901–910, 1995.
- Oppo, D. W., McManus, J. F., and Cullen, J. L.: Evolution and demise of the Last Interglacial warmth in the subpolar North Atlantic, *Quaternary Science Reviews*, 25, 3268–3277, 2006.
- Oppo, D. W., Curry, W. B., and McManus, J. F.: What do benthic $\delta^{13}\text{C}$ and $\delta^{18}\text{O}$ data tell us about Atlantic circulation during Heinrich Stadial 1?, *Paleoceanography*, 30, 353–368, 2015.
- Pahnke, K. and Zahn, R.: Southern Hemisphere water mass conversion linked with North Atlantic climate variability, *Science*, 307, 1741–1746, 2005.
- Paillard, D. and Parrenin, F.: The Antarctic ice sheet and the triggering of deglaciations, *Earth and Planetary Science Letters*, 227, 263–271, 2004.
- Peacock, S., Lane, E., and Restrepo, J. M.: A possible sequence of events for the generalized glacial-interglacial cycle, *Global Biogeochemical Cycles*, 20, 2006.
- Peterson, C. D., Lisiecki, L. E., and Stern, J. V.: Deglacial whole-ocean $\delta^{13}\text{C}$ change estimated from 480 benthic foraminiferal records, *Paleoceanography*, 29, 549–563, 2014.
- Raymo, M. E., Oppo, D. W., Flower, B. P., Hodell, D., McManus, J. F., Venz, K., Kleiven, K., and McIntyre, K.: Stability of North Atlantic water masses in face of pronounced climate variability during the Pleistocene, *Paleoceanography*, 19, 2004.
- Richter, T.: Sedimentary fluxes at the mid-atlantic ridge-sediment sources, accumulation rates, and geochemical characterisation, GEOMAR Report, GEOMAR Research Center for Marine Geosciences, Christian Albrechts University in Kiel, 73, 173, 1998.
- Ruddiman, W. F. and Ellis, E. C.: Effect of per-capita land use changes on Holocene forest clearance and CO₂ emissions, *Quaternary Science Reviews*, 28, 3011–3015, 2009.

- Rüggeberg, A., Dorschel, B., Dullo, W.-C., and Hebbeln, D.: Sedimentary patterns in the vicinity of a carbonate mound in the Hovland Mound Province, northern Porcupine Seabight, in: *Cold-water Corals and Ecosystems*, pp. 87–112, Springer, <https://doi.org/10.1594/PANGAEA.711998>, 2005.
- Sarnthein, M., Winn, K., Jung, S. J., Duplessy, J.-C., Labeyrie, L., Erlenkeuser, H., and Ganssen, G.: Changes in east Atlantic deepwater circulation over the last 30,000 years: Eight time slice reconstructions, *Paleoceanography*, 9, 209–267, 1994.
- Schmiedl, G. and Mackensen, A.: Late Quaternary paleoproductivity and deep water circulation in the eastern South Atlantic Ocean: Evidence from benthic foraminifera, *Palaeogeography, Palaeoclimatology, Palaeoecology*, 130, 43–80, 1997.
- Schmiedl, G. and Mackensen, A.: Multispecies stable isotopes of benthic foraminifera reveal past changes of organic matter decomposition and deepwater oxygenation in the Arabian Sea, *Paleoceanography*, 21, 2006.
- Schmitt, J., Schneider, R., Elsig, J., Leuenberger, D., Lourantou, A., Chappellaz, J., Köhler, P., Joos, F., Stocker, T. F., Leuenberger, M., et al.: Carbon isotope constraints on the deglacial CO₂ rise from ice cores, *Science*, 336, 711–714, 2012.
- Schmittner, A., Bostock, H. C., Cartapanis, O., Curry, W. B., Filipsson, H. L., Galbraith, E. D., Gottschalk, J., Herguera, J. C., Hoogakker, B., Jaccard, S., et al.: Calibration of the Carbon Isotope Composition ($\delta^{13}\text{C}$) of Benthic Foraminifera, *Paleoceanography*, 32, 512–530, 2017.
- Schönfeld, J., Zahn, R., and de Abreu, L.: Surface and deep water response to rapid climate changes at the Western Iberian Margin, *Global and Planetary Change*, 36, 237–264, 2003.
- Schweizer, M., Pawlowski, J., Kouwenhoven, T., and van der Zwaan, B.: Molecular phylogeny of common cibicidids and related Rotaliida (Foraminifera) based on small subunit rDNA sequences, *The Journal of Foraminiferal Research*, 39, 300–315, 2009.
- Shackleton, N.: Carbon-13 in *Uvigerina*: Tropical rainforest history and the equatorial Pacific carbonate dissolution cycles, *Marine science*, 1977.
- Shackleton, N., Le, J., Mix, A., and Hall, M.: Carbon isotope records from Pacific surface waters and atmospheric carbon dioxide, *Quaternary Science Reviews*, 11, 387–400, 1992.
- Shackleton, N., Hall, M., and Pate, D.: 15. Pliocene stable isotope stratigraphy of Site 846, in: *Proc. Ocean Drill. Program Sci. Results*, vol. 138, pp. 337–355, 1995.
- Shackleton, N. J., Imbrie, J., and Hall, M.: Oxygen and carbon isotope record of East Pacific core V19-30: implications for the formation of deep water in the late Pleistocene North Atlantic, *Earth and Planetary Science Letters*, 65, 233–244, 1983.
- Siegenthaler, U., Stocker, T. F., Monnin, E., Lüthi, D., Schwander, J., Stauffer, B., Raynaud, D., Barnola, J.-M., Fischer, H., Masson-Delmotte, V., et al.: Stable carbon cycle–climate relationship during the late Pleistocene, *Science*, 310, 1313–1317, 2005.
- Sigman, D. M. and Boyle, E. A.: Glacial/interglacial variations in atmospheric carbon dioxide, *Nature*, 407, 859–869, 2000.
- Sikes, E. L., Cook, M. S., and Guilderson, T. P.: Reduced deep ocean ventilation in the Southern Pacific Ocean during the last glaciation persisted into the deglaciation, *Earth and Planetary Science Letters*, 438, 130–138, 2016.
- Sikes, E. L., Allen, K. A., and Lund, D. C.: Enhanced $\delta^{13}\text{C}$ and $\delta^{18}\text{O}$ Differences Between the South Atlantic and South Pacific During the Last Glaciation: The Deep Gateway Hypothesis, *Paleoceanography*, 32, 1000–1017, 2017.
- Sirocko, F.: Abrupt change in monsoonal climate: evidence from the geochemical composition of Arabian Sea sediments, Ph.D. thesis, Christian-Albrechts-Universität zu Kiel, 1994.
- Sirocko, F., Sarnthein, M., Erlenkeuser, H., Lange, H., Arnold, M., and Duplessy, J. C.: Century-scale events in monsoonal climate over the past 24,000 years, *Nature*, 364, 322, 1993.

- Skinner, L. and Shackleton, N.: Rapid transient changes in northeast Atlantic deep water ventilation age across Termination I, *Paleoceanography*, 19, 2004.
- Skinner, L., Fallon, S., Waelbroeck, C., Michel, E., and Barker, S.: Ventilation of the deep Southern Ocean and deglacial CO₂ rise, *Science*, 328, 1147–1151, 2010.
- Skinner, L. C., Primeau, F., Freeman, E., de la Fuente, M., Goodwin, P., Gottschalk, J., Huang, E., McCave, I., Noble, T., and Scrivner, A.: Radiocarbon constraints on the glacial ocean circulation and its impact on atmospheric CO₂, *Nature communications*, 8, 16010, 2017.
- Slowey, N. C. and Curry, W. B.: Glacial-interglacial differences in circulation and carbon cycling within the upper western North Atlantic, *Paleoceanography*, 10, 715–732, 1995.
- Stern, J. V. and Lisiecki, L. E.: Termination 1 timing in radiocarbon-dated regional benthic $\delta^{18}\text{O}$ stacks, *Paleoceanography*, 29, 1127–1142, 2014.
- Stott, L. D., Neumann, M., and Hammond, D.: Intermediate water ventilation on the northeastern Pacific margin during the late Pleistocene inferred from benthic foraminiferal $\delta^{13}\text{C}$, *Paleoceanography*, 15, 161–169, 2000.
- Talley, L. D.: Closure of the global overturning circulation through the Indian, Pacific, and Southern Oceans: Schematics and transports, *Oceanography*, 26, 80–97, 2013.
- Tessin, A. and Lund, D.: Isotopically depleted carbon in the mid-depth South Atlantic during the last deglaciation, *Paleoceanography*, 28, 296–306, 2013.
- Thornalley, D. J., Elderfield, H., and McCave, I. N.: Intermediate and deep water paleoceanography of the northern North Atlantic over the past 21,000 years, *Paleoceanography*, 25, 2010.
- Tian, J., Wang, P., Cheng, X., and Li, Q.: Astronomically tuned Plio–Pleistocene benthic $\delta^{18}\text{O}$ record from South China Sea and Atlantic–Pacific comparison, *Earth and Planetary Science Letters*, 203, 1015–1029, 2002.
- Tjallingii, R., Claussen, M., Stuut, J.-B. W., Fohlmeister, J., Jahn, A., Bickert, T., Lamy, F., and Röhl, U.: Coherent high-and low-latitude control of the northwest African hydrological balance, *Nature Geoscience*, 1, 670, 2008.
- Toggweiler, J., Russell, J. L., and Carson, S.: Midlatitude westerlies, atmospheric CO₂, and climate change during the ice ages, *Paleoceanography*, 21, 2006.
- Vecsei, A. and Berger, W. H.: Increase of atmospheric CO₂ during deglaciation: constraints on the coral reef hypothesis from patterns of deposition, *Global Biogeochemical Cycles*, 18, 2004.
- Venz, K. A. and Hodell, D. A.: New evidence for changes in Plio–Pleistocene deep water circulation from Southern Ocean ODP Leg 177 Site 1090, *Palaeogeography, Palaeoclimatology, Palaeoecology*, 182, 197–220, 2002.
- Venz, K. A., Hodell, D. A., Stanton, C., and Warnke, D. A.: A 1.0 Myr record of Glacial North Atlantic Intermediate Water variability from ODP site 982 in the northeast Atlantic, *Paleoceanography*, 14, 42–52, 1999.
- Veum, T., Jansen, E., Arnold, M., Beyer, I., and Duplessy, J.-C.: Water mass exchange between the North Atlantic and the Norwegian Sea during the past 28,000 years, *Nature*, 356, 783, 1992.
- Voelker, A. H. and de Abreu, L.: A review of abrupt climate change events in the Northeastern Atlantic Ocean (Iberian Margin): Latitudinal, longitudinal, and vertical gradients, *Abrupt Climate Change: Mechanisms, Patterns, and Impacts*, pp. 15–37, 2011.
- Waelbroeck, C., Skinner, L., Labeyrie, L., Duplessy, J.-C., Michel, E., Vazquez Riveiros, N., Gherardi, J.-M., and Dewilde, F.: The timing of deglacial circulation changes in the Atlantic, *Paleoceanography*, 26, 2011.
- Wagner, M. and Hendy, I. L.: Trace metal evidence for a poorly ventilated glacial Southern Ocean, *Quaternary Science Reviews*, 170, 109–120, 2017.

- Wang, L., Sarnthein, M., Erlenkeuser, H., Grimalt, J., Grootes, P., Heilig, S., Ivanova, E., Kienast, M., Pelejero, C., and Pflaumann, U.: East Asian monsoon climate during the Late Pleistocene: high-resolution sediment records from the South China Sea, *Marine Geology*, 156, 245–284, 1999.
- Wei, G.-J., Huang, C.-Y., Wang, C.-C., Lee, M.-Y., and Wei, K.-Y.: High-resolution benthic foraminifer $\delta^{13}\text{C}$ records in the South China Sea during the last 150 ka, *Marine Geology*, 232, 227–235, 2006.
- Weinelt, M. and Sarnthein, M.: Stable isotope analysis on sediment core GIK11944-2, PANGAEA, doi: 10.1594/PANGAEA.97104 Reference (s): Weinelt, Mara (1993): Veränderungen der Oberflächenzirkulation im Europäischen Nordmeer während der letzten 60.000 Jahre-Hinweise aus stabilen Isotopen, *Berichte aus dem Sonderforschungsbereich 313*, Christian-Albrechts-Universität, Kiel, 41, 106, 2003.
- Weinelt, M., Vogelsang, E., Kucera, M., Pflaumann, U., Sarnthein, M., Voelker, A., Erlenkeuser, H., and Malmgren, B.: Variability of North Atlantic heat transfer during MIS 2, *Paleoceanography*, 18, 2003.
- Woodruff, F. and Chambers, S.: Middle Miocene benthic foraminiferal oxygen and carbon isotopes and stratigraphy: southern ocean site 744, in: *Proc. ODP Sci. Results*, vol. 119, pp. 935–939, 1991.
- Woodruff, F. and Savin, S. M.: $\delta^{13}\text{C}$ values of Miocene Pacific benthic foraminifera: Correlations with sea level and biological productivity, *Geology*, 13, 119–122, 1985.
- Xu, J., Holbourn, A., Kuhnt, W., Jian, Z., and Kawamura, H.: Changes in the thermocline structure of the Indonesian outflow during Terminations I and II, *Earth and Planetary Science Letters*, 273, 152–162, 2008.
- Yu, J., Anderson, R., and Rohling, E.: Deep ocean carbonate chemistry and glacial-interglacial atmospheric CO_2 changes, *Oceanography*, 2014.
- Zahn, R. and Stüber, A.: Suborbital intermediate water variability inferred from paired benthic foraminiferal Cd/Ca and $\delta^{13}\text{C}$ in the tropical West Atlantic and linking with North Atlantic climates, *Earth and Planetary Science Letters*, 200, 191–205, 2002.
- Zahn, R., Winn, K., and Sarnthein, M.: Benthic foraminiferal $\delta^{13}\text{C}$ and accumulation rates of organic carbon: *Uvigerina peregrina* group and *Cibicidoides wuellerstorfi*, *Paleoceanography*, 1, 27–42, 1986.
- Zarriess, M. and Mackensen, A.: Testing the impact of seasonal phytodetritus deposition on $\delta^{13}\text{C}$ of epibenthic foraminifer *Cibicidoides wuellerstorfi*: A 31,000 year high-resolution record from the northwest African continental slope, *Paleoceanography*, 26, 2011.
- Zhang, J., Wang, P., Li, Q., Cheng, X., Jin, H., and Zhang, S.: Western equatorial Pacific productivity and carbonate dissolution over the last 550 kyr: Foraminiferal and nannofossil evidence from ODP Hole 807A, *Marine Micropaleontology*, 64, 121–140, 2007.